Article

Cell Reports

Functional Plasticity of Odor Representations during Motherhood

Graphical Abstract

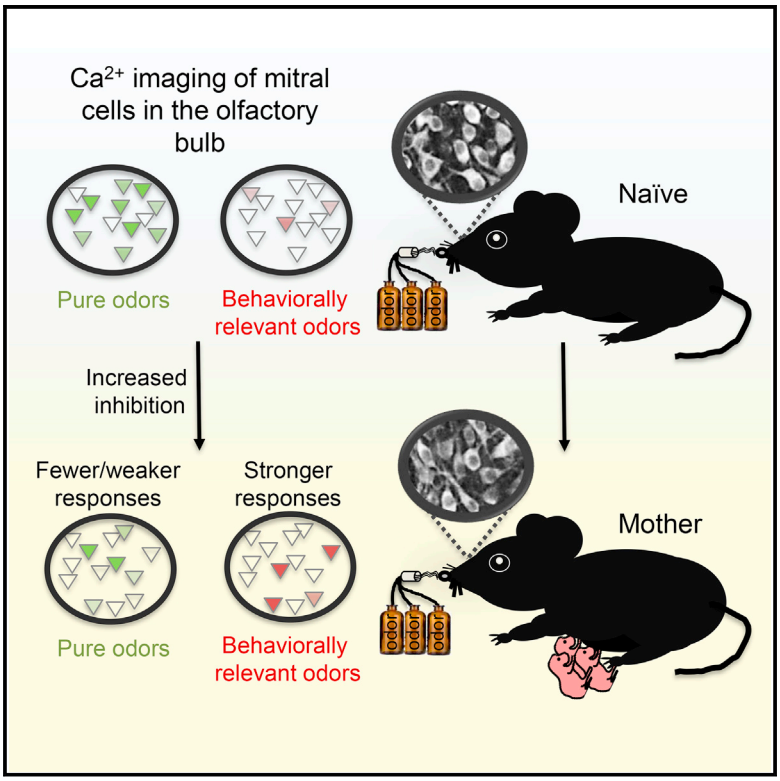

Authors

Amit Vinograd, Yael Fuchs-Shlomai, Merav Stern, ..., Ami Citri, Ian Davison, Adi Mizrahi

Correspondence

mizrahi.adi@mail.huji.ac.il

In Brief

Motherhood is associated with changes in neural circuits that affect how the mother senses her surroundings. Vinograd et al. show that the olfactory bulb is a locus of plasticity. Output neurons of the bulb have elevated inhibition, and odor coding of natural odors is improved.

Highlights

- MCs of mothers show sparser responses for pure odors
- MCs of mothers have stronger inhibitory drive onto MCs
- MCs of mothers show stronger responses to natural odors
- MC ensemble coding is improved for natural but not pure odors

Vinograd et al., 2017, Cell Reports *21*, 351–365
October 10, 2017
https://doi.org/10.1016/j.celrep.2017.09.038

CellPress

Cell Reports
Article

Functional Plasticity of Odor Representations during Motherhood

Amit Vinograd,[1,3,6] Yael Fuchs-Shlomai,[1,3,6] Merav Stern,[4] Diptendu Mukherjee,[2,3] Yuan Gao,[5] Ami Citri,[2,3] Ian Davison,[5] and Adi Mizrahi[1,3,7,*]
[1]Department of Neurobiology
[2]Department of Chemical Biology, Institute of Life Sciences
[3]The Edmond and Lily Safra Center for Brain Sciences
The Hebrew University of Jerusalem, Edmond J. Safra Campus, Jerusalem 91904, Israel
[4]Department of Applied Mathematics, University of Washington, Seattle, WA, USA
[5]Department of Biology, Boston University, Boston, MA, USA
[6]These authors contributed equally
[7]Lead Contact
*Correspondence: mizrahi.adi@mail.huji.ac.il
https://doi.org/10.1016/j.celrep.2017.09.038

SUMMARY

Motherhood is accompanied by new behaviors aimed at ensuring the wellbeing of the offspring. Olfaction plays a key role in guiding maternal behaviors during this transition. We studied functional changes in the main olfactory bulb (OB) of mothers in mice. Using in vivo two-photon calcium imaging, we studied the sensory representation of odors by mitral cells (MCs). We show that MC responses to monomolecular odors become sparser and weaker in mothers. In contrast, responses to biologically relevant odors are spared from sparsening or strengthen. MC responses to mixtures and to a range of concentrations suggest that these differences between odor responses cannot be accounted for by mixture suppressive effects or gain control mechanisms. In vitro whole-cell recordings show an increase in inhibitory synaptic drive onto MCs. The increase of inhibitory tone may contribute to the general decrease in responsiveness and concomitant enhanced representation of specific odors.

INTRODUCTION

The transition to motherhood is a dramatic event that is accompanied by the emergence of maternal behaviors to enhance parental reproductive success. Maternal care and protection are hallmarks of many species and are particularly prominent in mammals (Dulac et al., 2014). In mice, for example, maternal behaviors are reflected in nest building, pup retrieval and licking, heightened alertness, and aggression toward intruders. Such behavioral changes are most likely associated with plastic changes in specific neuronal circuits across the brain, but these are not well characterized.

Multiple brain regions have been implicated in controlling maternal behaviors, including the amygdala, the hypothalamus, and the nucleus accumbens (Numan, 2006; Poindron, 2005; Wu et al., 2014; Zilkha et al., 2017). Changes in these brain regions are most likely a result of the combined effects of intrinsic (endocrine) and extrinsic (environmental) factors. Sensory systems are likely to be nodes of plasticity because the information conveyed by them to downstream targets is behaviorally salient. Olfaction, audition, and somatosensation are particularly relevant for maternal changes because sensory cues and contingencies, which arise from the novel environment of mothers, are carried by these senses (Elyada and Mizrahi, 2015).

The olfactory system has been shown to be essential in plasticity paradigms like enrichment and learning (Chu et al., 2016; Gschwend et al., 2015) as well as for the early interactions between the mother and offspring (Lévy and Keller, 2009; Poindron, 2005; Dulac et al., 2014). Accumulating evidence suggests that the olfactory bulb (OB) in mothers is a primary site of plasticity. For example, several studies have described plasticity of neuromodulatory circuits as well as local circuits in the OB following parturition (Dickinson and Keverne, 1988; Kopel et al., 2012; Shingo et al., 2003; Lévy et al., 1990; Kendrick et al., 1992). Moreover, a study performed in sheep showed that the OB output neurons, the mitral cells (MCs), undergo marked changes in their responsiveness to the scent of their offspring versus the scent of food after parturition (Kendrick et al., 1992). Recent years have seen an increase in our understanding of odor processing in the OB under normal conditions (Uchida et al., 2014; Murthy, 2011a; Schaefer and Margrie, 2007), paving the way for a better mechanistic understanding of how the bulbar circuitry is involved in maternal plasticity.

Here we asked whether and to what extent odor processing of general (non-salient) monomolecular odors and behaviorally relevant (salient) odors changes in mothers.

RESULTS

To explore functional changes in the OB following parturition, we compared the odor response profiles of MCs in naive females with those of age-matched primiparous lactating mothers 3–5 days after parturition. We imaged MCs using in vivo two-photon calcium imaging in transgenic mice expressing the genetically encoded calcium indicator GCaMP3 under the

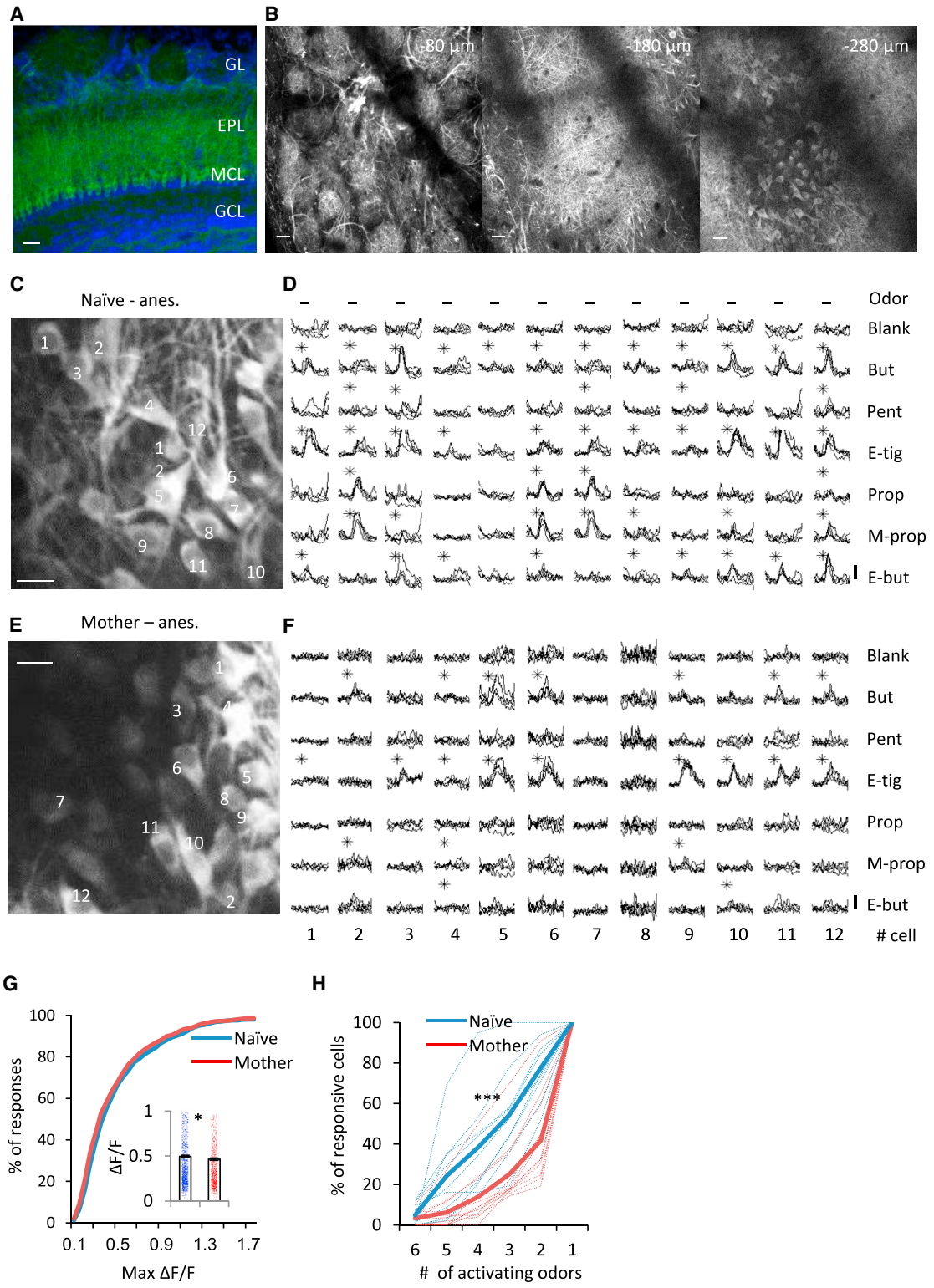

Figure 1. MC Response Profiles Become Sparse Following the Transition to Motherhood

(A) Confocal micrograph of labeled MCs in a Thy1-GCaMP3 mouse. GL, glomerular layer; EPL, external plexiform layer; MCL, mitral cell layer; GCL, granule cell layer. Scale bar, 70 µm.

(B) In vivo two-photon micrographs of a Thy1-GCaMP3 mouse showing GCaMP3 labeling at −80, −180, and −280 µm from the dura. Scale bars, 70 µm.

(legend continued on next page)

Thy1 promoter (Chen et al., 2012; Figures 1A and 1B). GCaMP3 was previously shown to be a reliable reporter of spiking activity in various brain regions, including the OB (Akerboom et al., 2012; Chen et al., 2012; Kato et al., 2012; Tian et al., 2009; Wachowiak et al., 2013). To characterize the responsiveness of MCs to general odors, we presented to anesthetized naive females or mothers a panel of 6 pure odorants that activate the dorsal surface of the OB (Figures 1C and 1D, naive females; Figures 1E and 1F, mothers; Adam et al., 2014; Livneh et al., 2014). GCaMP fluorescence values (ΔF/F) were normally stable throughout an experiment, and calcium transients in response to odor stimulation were reliable across trials (Figures 1D and 1F). Calcium responses to the different odors were heterogeneous across the MC population. All six odors normally induced calcium responses at one or multiple fields.

MC Response Profiles Become Sparser following the Transition to Motherhood

Brief (2-s) odor stimulation readily evoked robust GCaMP responses in the MCs of naive females. 83% of MCs responded to at least one odor in our stimulus set (n = 10 mice, 1,348 cells). In contrast, odor responses in MCs of mothers were substantially sparser. Only 37.8% of MCs from mothers responded to at least one odor (n = 12 mice, 2,178 cells). Notably, the peak amplitude of odor-evoked calcium transients per cell was reduced in mothers (mean ± SEM; naive females, 0.50 ± 0.01; mothers, 0.46 ± 0.01; p = 0.01; Mann-Whitney *U* test; Figure 1G). To further quantify the changes in MC response profiles, we scored their odor selectivity by plotting the number of odors activating each odor-responsive neuron. Individual MCs of naive females responded to significantly more odors compared with MCs of mothers (Kolmogorov-Smirnov test, $p = 6.6x10^{-18}$). More than half of the MCs in mothers (58.3%) responded to only a single odor, whereas, in naive females, only 22.5% showed such high selectivity (Figure 1H). The reduced responsiveness of MCs in mothers was also evident when the data were analyzed per odor. Each of the 6 odors drove responses from fewer MCs in mothers (Figure S1C; binomial proportion test, for all odors p < 0.001). These data show that MCs become more selective for this set of pure odors.

Temporal dynamics have been shown to be important for odor coding. Thus, we tested MC responses to persistent odor stimuli (15 s, n = 6 mice, 529 cells in naive females and n = 9 mice, 1,385 cells in mothers). Although evoked responses were diverse, we found a strong effect on the ''latency'' and ''time to peak'' of odor responses, both of which were delayed in mothers (Figures S2B and S2D–S2H). Thus, general odor responses in mothers are not only weaker and fewer but also slower to evolve.

Sparsening of MC Response Profiles in Mothers Persists in the Awake State

Anesthesia has been shown to increase responsiveness in the OB (Kato et al., 2012; Rinberg et al., 2006). Thus, we examined whether the response profile of MCs in mothers show similar differences in the awake state as well (Figures 2A and 2B, naive females; Figures 2C and 2D, mothers). Consistent with the results in anesthetized mice, the mean peak amplitude of odor-evoked responses was lower in mothers (Figure 2E), and MC responses were again sparser (Figure 2F; 44% and 39% responsive MCs in naive females and mothers, respectively). As expected from previous reports, MC activity in naive mice was weaker in the awake state (Figure 2G). Notably, MCs in mothers were also affected by anesthesia, but to a lesser extent (Figure 2G; Figure S1; general responsiveness numbers). This result supports our findings of reduced odor-evoked responses in mothers.

The sparsening effect we observed under anesthesia was weaker in the awake state (compare Figure 1H with Figure 2F). Thus, to further strengthen our claim about sparsening of these particular odors in motherhood, we conducted a time lapse experiment. Using chronic imaging, we imaged the exact same cells before and after parturition in awake mice (Figures S3A–S3C; n = 2 mice; n = 193 cells). Consistent with the data above, we found an overall decrease in response magnitude and the total number of odors to which each MC responded (Figures S3D–S3G).

Behaviorally Relevant Odors Are Spared from Sparsening in Mothers

Next we expanded our odor set to other odors that are behaviorally salient. To this end, in a subset of naive females (n = 4 anesthetized mice, 819 cells; n = 4 awake mice, 379 cells) and mothers (n = 4 anesthetized mice, 793 cells; n = 4 awake mice, 408 cells), we examined MC responses to behaviorally relevant odors. Our odor set included male mouse urine, female mouse urine, and peanut butter, which have been shown in previous studies to elicit attraction in mice; trimethylthiazoline (TMT), which was documented to elicit aversive behavior (Root et al., 2014; Kobayakawa et al., 2007); and nest odors.

Surprisingly, MCs in mothers showed a general trend of increased responsiveness to this odor set (Figures 3A and 3B) rather than the decrease predicted by our initial results. Individual MCs in mothers responded to a greater number of natural odors compared with naive females (Figure 3E; 46% and 48% responsive MCs in naive females and mothers, respectively) and showed higher values of peak amplitudes (naive females, 0.26 ± 0.01; mothers, 0.33 ± 0.01; Mann-Whitney *U* test;

(C) Two-photon micrograph of a representative field used for imaging in a naive female. Anes., anesthetized. Scale bar, 20 μm.
(D) Calcium transients elicited by the 12 neurons in the field shown in (C) in response to a 2-s odor stimulation with 6 monomolecular odors. Each trace represents a single trial. Black asterisks denote statistically significant responses. Vertical bar, 25% ΔF/F.
(E and F) As in (C) and (D), but data were collected from a mother.
(G) Cumulative distribution of peak odor-evoked responses in naive females (blue) and in mothers (red). Inset: mean ± SEM peak amplitude of odor-evoked calcium transients per cell in naive females (blue) and mothers (red) (*p < 0.05, Mann-Whitney *U* test).
(H) Cumulative distribution of the percentages of MCs responding to 1–6 odors in naive females (blue) and in mothers (red). Each dashed line represents an individual mouse (***p < 0.0001, Kolmogorov-Smirnov test).

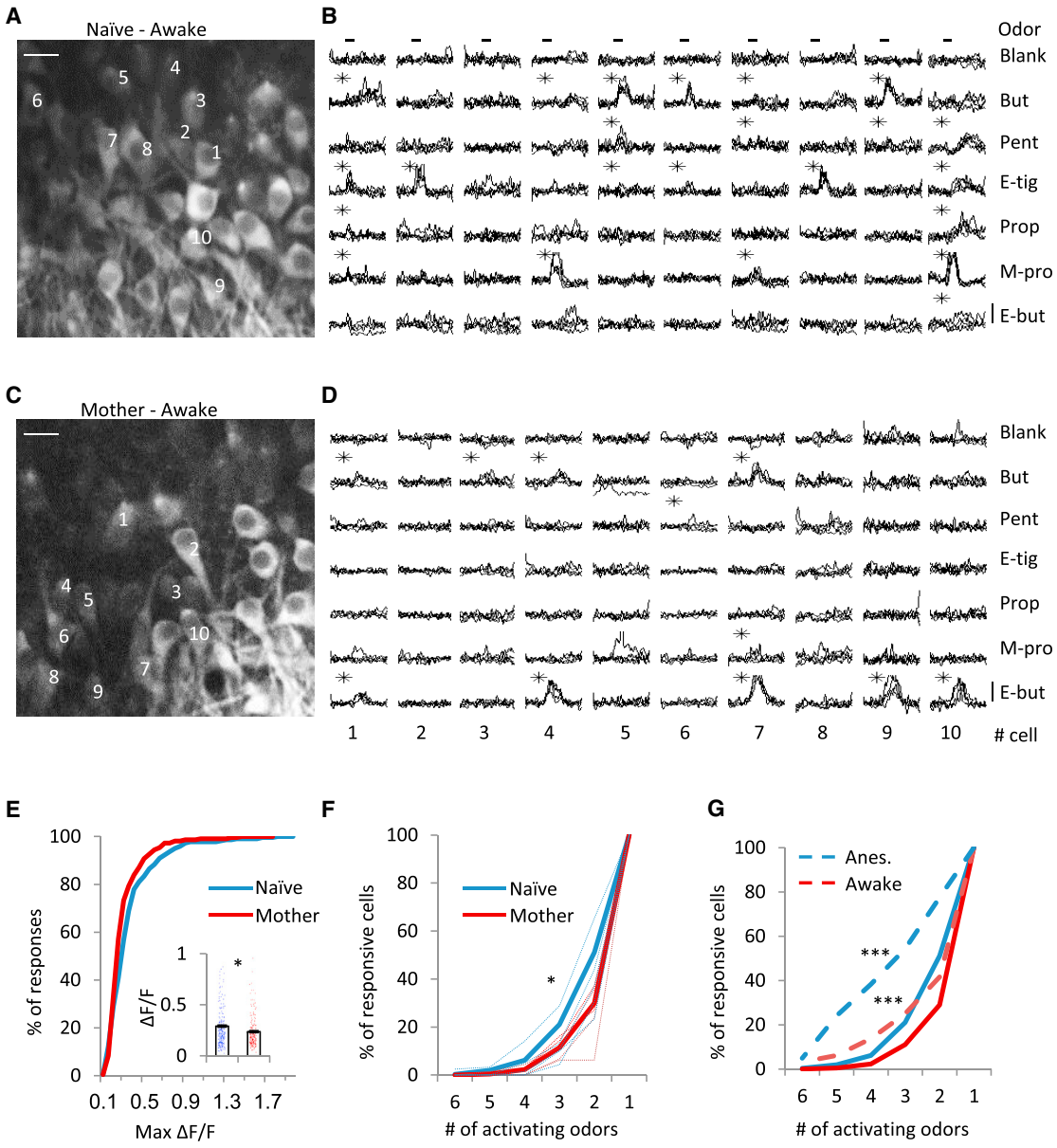

Figure 2. Sparsening of MC Response Profiles in Mothers Persists in the Awake State

(A–F) The same as Figures 1C–1H for awake mice. Scale bars, 20 μm (A and C). Vertical bars, 25% ΔF/F (B and D). *p < 0.05, Mann-Whitney *U* test (E); *p < 0.05, Kolmogorov-Smirnov test (F).

(G) Comparison of average MC selectivity between the awake (solid lines) and anesthetized states (dashed lines), the same data as shown in Figure 1H and in (F) (***p < 0.0001, Kolmogorov-Smirnov test).

p = 0.008; Figure 3E). Notably, although natural odors induced similar or larger responses in mothers versus naive females, these constituted smaller effects compared with the pure odors (Figure S1B). However, comparing the relative responses to pure versus natural odors within a group showed that motherhood induced an inhibitory effect to pure odors and, concomitantly, a weak positive effect to natural odors (Figure S1). This general trend of being spared from sparsening was similar in awake mice (Figures 3G and 3H; Figure S1).

Differential Maternal Plasticity Is Not due to Differences in Mixture Suppression or Gain Control Mechanisms

There are several potential explanations for the differential effects of motherhood on "pure" versus "biologically relevant" odors. The natural odors are mostly mixture blends, which may be processed differently by main olfactory bulb (MOB) circuits, and were also presented undiluted, raising the possibility of concentration-dependent effects. Leveraging the robust responses to pure odors and the ability to manipulate them with precision,

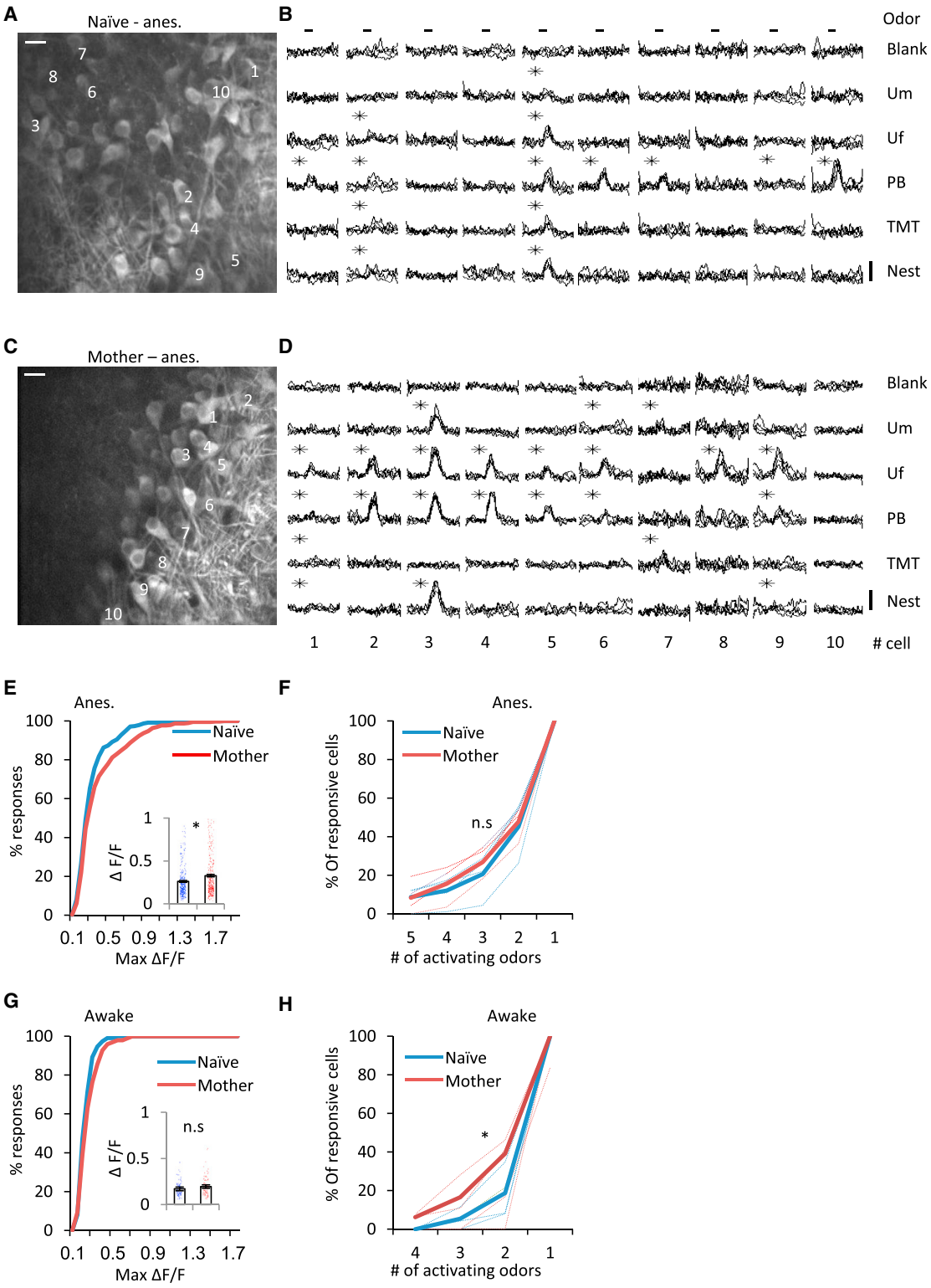

Figure 3. MCs in Mothers Show Increased Responsiveness to Natural Odors

(A–H) The same as Figures 1C–1H for natural odors. Imaging traces are from anesthetized mice. Scale bars, 20 μm (A and C). Vertical bars, 25% ΔF/F (B and D). (E and F) Anesthetized mice. (G and H) Awake mice. (E and G) *p < 0.05, Mann-Whitney U test. (F and H) *p < 0.05, Kolmogorov-Smirnov test). Um, male urine; Uf, female urine; PB, peanut butter; TMT, trimethylthiazoline; Nest, pup + nest.

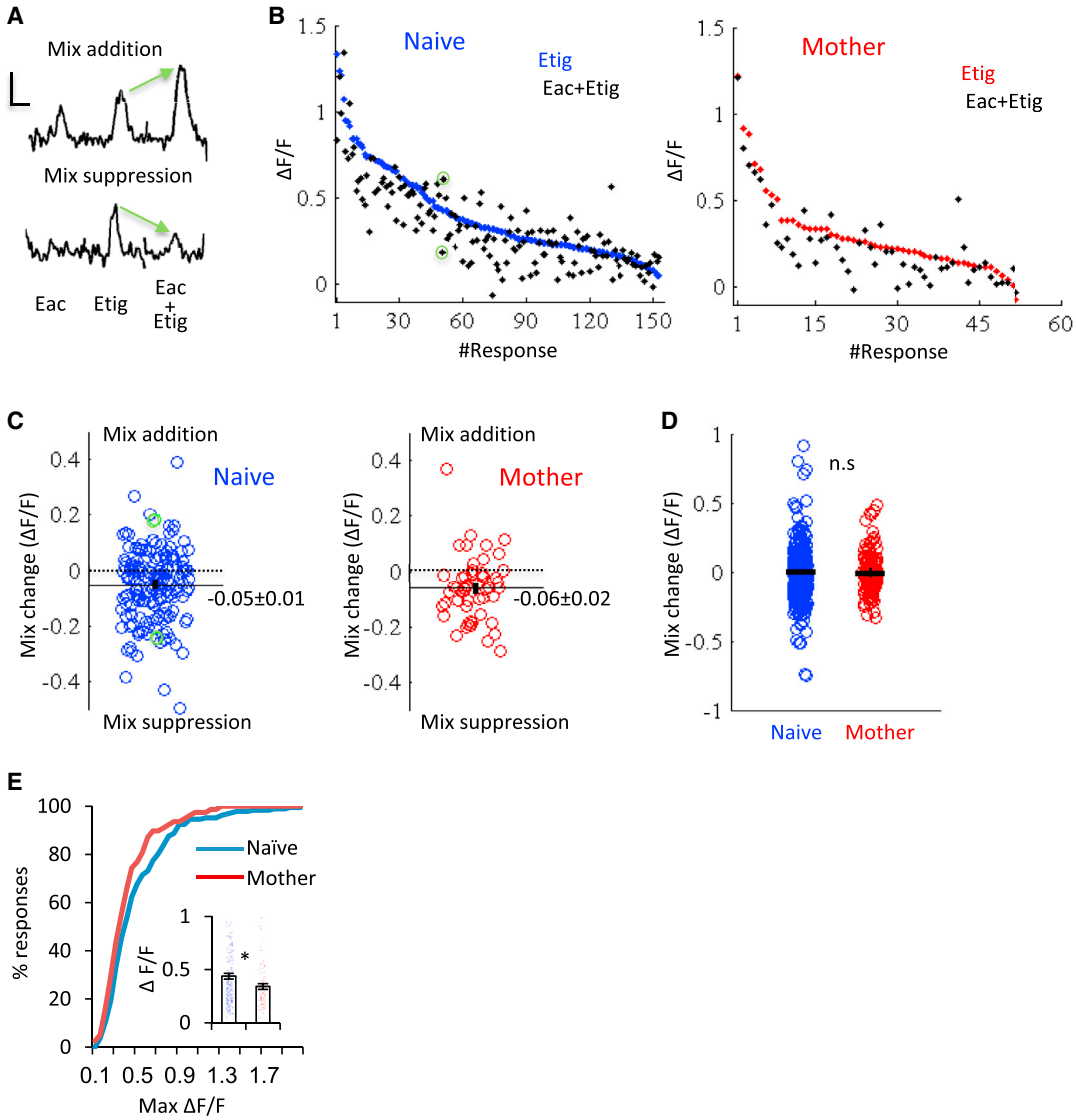

Figure 4. Similar Mixture Processing in Naive Females and Mothers

(A) Example of 2 MC responses to two odors and their mixtures (average of 4 trials). Top cell, mixture addition; bottom cell, mixture suppression. Etig, ethyl tiglate; Eac, ethyl acetate. Scale bars, 5 s, 25% ΔF/F.

(B) Left: MC responses from naive females to Etig (blue, sorted by amplitude) and the responses of the same MC to the mixture (black, Etig + Eac). Green circles correspond to the MC in (A). Right: MC responses to Etig and Eac + Etig mixture in mothers.

(C) Changes in ΔF/F (mean ± SEM) from odor responses to the mixture responses shown in (B). Green circles correspond to the MC in (A) and (B).

(D) Changes in ΔF/F (mean ± SEM) between all odor mixture combinations (see Experimental Procedures for details). p = 0.6, Mann-Whitney *U* test.

(E) Cumulative distribution of peak odor-evoked responses in naive females (blue) and in mothers (red) for the subset of mice used for the mixture experiments (n = 3 naive females, 3 mothers). Inset: mean ± SEM peak amplitude of odor-evoked calcium transients per cell in naive females (blue) and mothers (red) (*p < 0.05, Mann-Whitney *U* test).

we tested these questions with pure odor mixtures and different concentrations.

We tested mixture interaction effects in naive females and mothers (n = 3 naive females, 500 cells; 3 mothers, 335 cells). We compared the responses of odors presented in isolation and as binary mixtures. The responses to mixtures were heterogeneous, showing a full spectrum of responses from mixture addition to mixture suppression (Figures 4A and 4B). The majority of responses to mixtures were suppressive, and this was similar in naive females and mothers (Figures 4B and 4C). Note that, although the average responses in mothers were still weaker compared with naive females, the mixture effects were statistically indistinguishable (Figures 4C–4E). These data suggest that differences in MC responses to natural odors in mothers were not due to the fact that they were mixture blends.

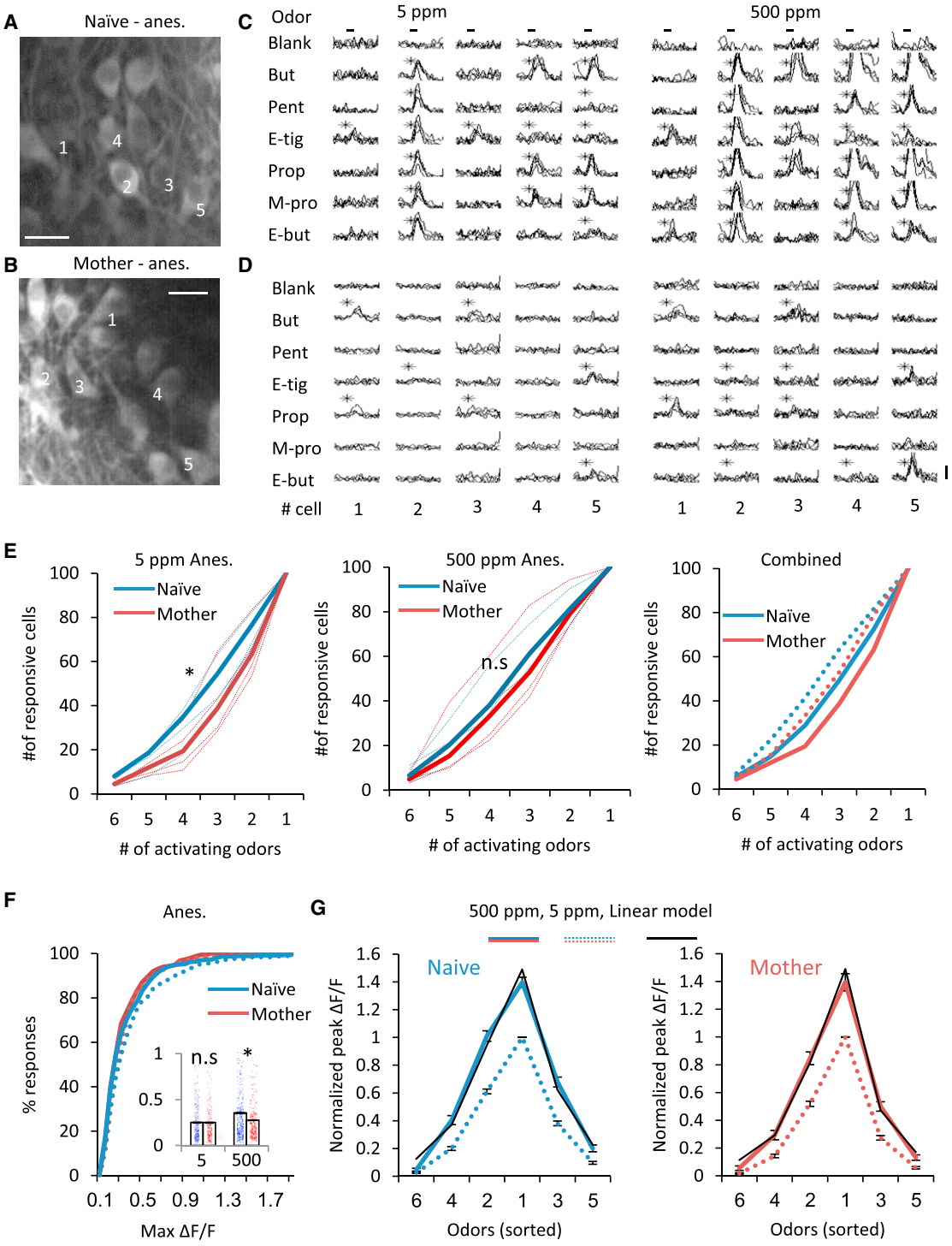

Figure 5. Similar Processing of Odor Concentrations in Naive Females and Mothers

(A and B) Two-photon micrograph of a representative field used for imaging in a naive female (A) and a mother (B). Scale bars, 20 μm.

(C and D) Calcium transients elicited by the neurons in the field shown in (A) and (B) (cells marked by numbers in A and B) in response to a 5-ppm odor concentration (left) and 500 ppm (right). Each line represents a single trial. Black asterisks denote statistically significant responses. Vertical bars, 25% ΔF/F.

(E) Cumulative distribution of the percentage of MCs responding to 1–6 odors in naive females (blue) and in mothers (red). Each dashed line represents an individual mouse. Left:5 ppm; center, 500 ppm; right, 5 ppm (solid lines) and 500 ppm (dashed lines) combined. *$p < 0.05$, Kolmogorov-Smirnov test.

(F) Cumulative distribution of peak odor-evoked responses in naive females (blue) and in mothers (red). 5 ppm (solid lines) and 500 ppm (dashed lines). Inset: mean ± SEM peak amplitude of odor-evoked calcium transients per cell in 5 ppm and 500 ppm. *$p < 0.05$, Mann-Whitney *U* test.

(legend continued on next page)

Next we tested odor responses in naive females and mothers (n = 4 naive females, 461 cells; 4 mothers, 420 cells) to a difference in concentration of two orders of magnitude (5 ppm and 500 ppm) (Figures 5A and 5B). The maternal sparsening of odor-evoked responses was again evident in these experiments. However, there were slight quantitative differences compared with the responses to the 50 ppm odors shown above. Specifically, under the lower odor concentration condition, responses in mothers were sparser but not weaker (Figures 5E and 5F; responsiveness: naive females, 38%; mothers, 30%). Under the high odor concentration condition, the responses had similar sparseness but weaker peak responses (Figures 5E and 5F; responsiveness: naive females, 42%; mothers, 39%). Because low and high odor concentrations were tested on a per-neuron basis, we could evaluate the direct changes in responsiveness as a result of concentration, adapting the gain control analysis carried out by Kato et al., 2013. Both naive mice and mothers show a perfect fit to the exact same linear transformation in the transition from low to high odor responses, suggesting that gain control mechanisms operate similarly in both experimental groups. The experiments confirm that responses are sparsened across a range of concentrations and also rule out the explanation that differences between natural and pure odor plasticity are due to changes in how the OB processes mixtures or concentrations.

Direct Synaptic Inhibition onto MCs Is Upregulated in Mothers

A robust effect we routinely measured in the different experiments is a generally weaker or sparser MC response to pure odors (Figures 1, 2, 4, and 5; Figures S1–S3). One possible way of accounting for these responses in mothers is elevated synaptic inhibition onto MCs. Thus, we next measured GABAergic inputs received by MCs in naive females and mothers. First, we made whole-cell recordings from MCs in brain slices taken from naive females and mothers and measured miniature inhibitory postsynaptic currents (mIPSCs) isolated by incubation with tetrodotoxin (TTX), 2,3-dihydroxy-6-nitro-7-sulfamoyl-benzo[F]quinoxaline-2,3-dione (NBQX), and (2*R*)-amino-5-phosphonopentanoate (APV) (Figures 6A and 6B; 1 μM, 5 μM, and 50 μM, respectively). The mean amplitude of mIPSCs was indistinguishable between the groups (Figures 6C–6E; naive females, n = 14 cells in 4 mice; mothers, n = 15 cells in 4 mice). However, mIPSC frequency was greatly increased in mothers, by approximately 2-fold (Figures 6F and 6G). These data suggest either a change in presynaptic components and/or the addition of new synapses to inhibitory circuits in the OB.

We also examined the relative contribution of synaptic inhibition to responses evoked by stimulating the olfactory nerve adjacent to the MC parent glomerulus (n = 8 cells in 5 mothers, n = 5 cells in 3 naive mice). At reversal potential for inhibitory currents (−75 mV), olfactory nerve layer stimulation evoked a long-lasting inward current reflecting both monosynaptic input from the olfactory nerve and intraglomerular excitation from other MCs (Figure 6H; Gire et al., 2012; Carlson et al., 2000). Our stimulation parameters generated similar excitatory input in naive females and mothers (quantified either as peak current or integrated charge). The magnitude of inhibitory currents measured at +5 mV, however, was dramatically increased in mothers. Because complete reversal of excitatory input was prevented by local coupling between MCs (Gire et al., 2012), we quantified the excitatory-inhibitory balance as an index reflecting the product of amplitude and frequency of individual outward currents (rather than the integral of amplitude or charge; Figure 6H, inset, arrowheads). This revealed that the ratio of inhibition to excitation was greatly and significantly increased in mothers (Figure 6I).

Our findings of increased inhibition in the OB following parturition were further corroborated by evaluating the levels of RNA expression of molecules associated with inhibitory synapses. We observed a consistent and significant upregulation of GAD1, Gephyrin, and the delta subunit of the gamma-aminobutyric acid-A (GABAA) receptor in OBs from mothers in comparison with naive females. Expression of GAD1 and Gephyrin increased on average by 65% and 35%, respectively (Figures S4A and S4B) (t test; $p < 0.001$ and $p < 0.01$, respectively). The GABAA-delta subunit also increased, but more modestly (Figures S4A and S4B; t test, $p = 0.026$). Importantly, the strong transcriptional induction of GAD1 and Gephryin was consistent across all individual bulbs tested (Figure S4A). GAD1 is a gamma-aminobutyric acid (GABA) biosynthetic enzyme, whereas Gephyrin acts postsynaptically to localize and stabilize GABA receptors at the postsynaptic membrane. These results therefore indicate that both presynaptic as well as postsynaptic enhancement of GABA transmission may be occurring within OB of mothers.

Improved Coding of Natural Odors in Mothers

Finally, to evaluate coding in response to the different odor sets more directly, in a subset of anesthetized mice, we collected responses from MCs that were stimulated by all 11 odors, including 6 pure odors and 5 natural odors (n = 4 naive females, n = 819 MCs; n = 4 mothers, n = 793 MCs). In both mothers and naive females, the responses of single cells to pure odors were stronger than to natural odors, but the responses to natural odors were stronger compared with naive females (Figure 7A). By normalizing the maximum response of the cell to all 11 odors tested, the increase in the relative response to natural odors was also higher in mothers ($p = 0.0002$, Mann-Whitney *U* test; Figure 7B). To test how consistent the response of neurons in the OB is, we calculated pairwise signal correlations among neighboring neurons from the same mice (Figures 7C and 7D). Interestingly, signal correlations in mothers increased for pure odors but decreased for natural odors (Figure 7E). This

(G) Gain control analysis for the transition from 5 ppm to 500 ppm odor-evoked responses. Odors were ranked for each cell according to the response amplitude during 5-ppm trials, and the same order was kept for each cell in the 500-ppm trials. The tuning curves are averaged across all cells from 5 ppm (naive female and mother, blue and red dotted lines, respectively) and 500 ppm (blue and red solid lines) that showed responses to at least one of six tested odors (n = 4 naive females, 382 MCs; 4 mothers, 343 MCs). The black line represents a curve based on the same linear transformation (1.40 × 5 ppm response + 0.09) both for naive females and mothers.

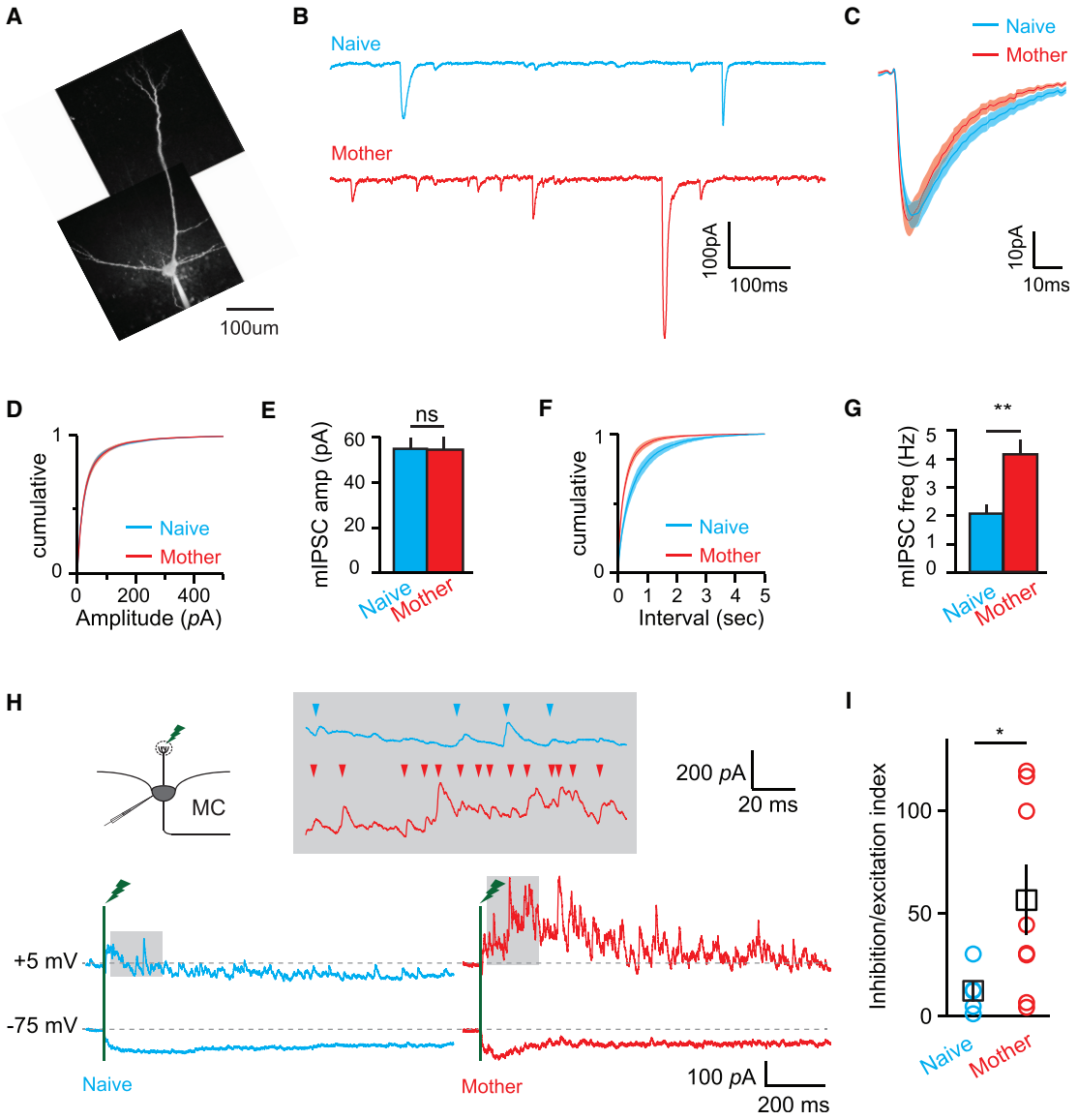

Figure 6. Whole-Cell Slice Recordings Show Increased mIPSCs onto MCs of Mothers

(A) An MC filled with fluorescent dye during recording.

(B) Pharmacologically isolated mIPSCs recorded from naive females (top, blue) and mothers (red, bottom).

(C) Average ± SEM of all mIPSC events from naive females and mothers.

(D and E) Cumulative histograms (D) and averages ± SEM for mIPSC amplitudes (C) in naive females and mothers. Amplitudes were not significantly different in both groups (47.4 ± 3.6 pA and 54.9 ± 4.7 pA for mothers and naive females, respectively; $p > 0.2$, t test).

(F and G) Cumulative histograms of inter-event interval (F) and averages of mean ± SEM mIPSC frequency (G). The frequency was greatly increased in mothers (4.1 ± 0.6 Hz versus 2.1 ± 0.3Hz; $^{**}p < 0.01$, t test).

(H) Synaptic currents evoked by stimulation of the olfactory nerve.

(I) Average ± SEM of the ratio of inhibition to excitation. Inhibition/excitation (I/E) ratios were significantly enhanced in mothers compared with naive females (56.39 ± 16.98 versus 12.25 ± 5.01, respectively; $^{*}p < 0.05$, t test).

suggests that mothers have a more redundant population code for pure odors and a less redundant representation for natural odors.

To analyze how MC ensembles compute different odors in the OB of mothers versus naive females, we described each population response to one odor in each mouse as a vector with a given angle and size (illustrated in Figure 7F; $\vec{a}$, $\vec{b}$, $\vec{c}$), where each element represents the response of each MC to that odorant. We assessed the similarity in population responses to distinct odors quantitatively using Euclidean distances and cosine similarities (Figures 7F–7H, top and bottom, respectively) and qualitatively using principle-component analysis (PCA).

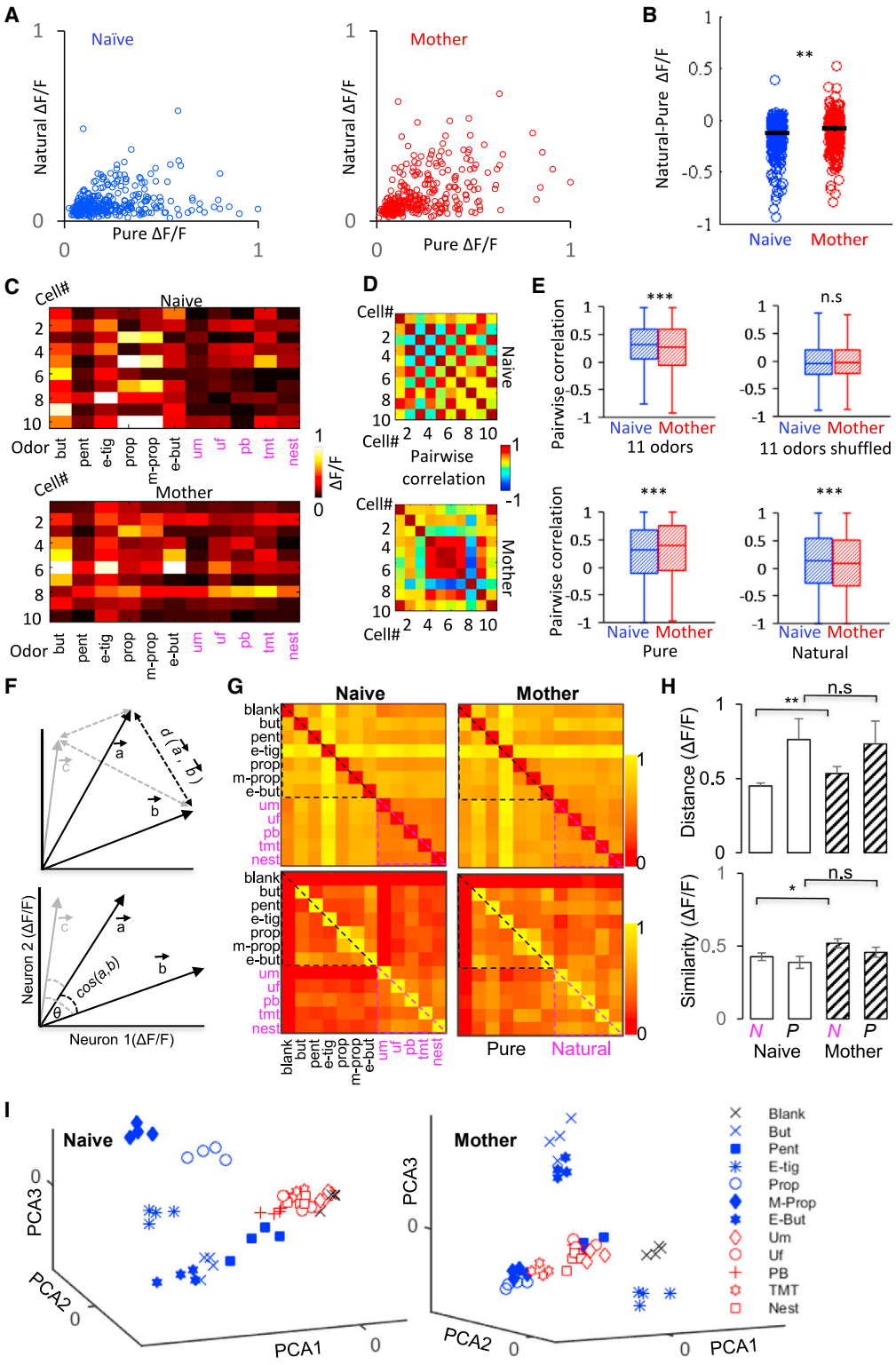

Figure 7. Pairwise Correlations Carry More Information to Natural Odors

(A) Scatterplots of maximum response amplitudes in individual MCs responding to both natural and pure odors, normalized to the maximum response. Blue, naive females; red, mothers.

(B) Scatterplot of the difference in calcium response to natural and pure odors in all cells responding both to pure and natural odors (**$p < 0.001$, Mann-Whitney *U* test). The line marks the mean ± SEM.

(legend continued on next page)

The pairwise Euclidean distance values between all odor pairs clearly shows that the stronger responses elicited by pure odors are better separated from natural odors that evoked a weaker response (Figure 7G, top). The normalized average distance for pure odors was higher compared with natural odors in the naive females group (0.76 compared with 0.45, a ratio of 0.59). Interestingly, mothers showed an increase in the distances between natural odors but no change in the distances between pure odors, considerably attenuating this ratio from 0.59 in naive females to 0.73 in mothers (Figures 7G and 7H, top). Cosine similarity analysis of the same data complemented the distance analysis. The average cosine similarity of pure odor responses was not different between mothers and naive females, and natural odors were slightly higher in mothers (Figures 7G and 7H, bottom). This suggests that the increased separation of natural odors in mothers can more likely be contributed by changes in response amplitudes. PCA, which provides a good visual representation of the results, showed that MC population ensembles separate pure odors better compared with natural odors in both groups (Figure 7I). Notably, however, and in agreement with the vector analysis, the responses to natural odors are better separated from the blank and among this group of odors in mothers (Figure 7I).

In summary, mothers have a distinct profile of neural representations for different types of odorants. Despite the sparser responses in mothers to pure odors, the population similarity was neither improved nor deteriorated. Natural odors, however, which show increased responsiveness in mothers, have better separation by the populations of MCs compared with the pure odor set, suggesting a substrate for improved coding of natural odors in mothers.

DISCUSSION

Distinct Changes to Different Odors

In search for neuronal circuits involved in the repertoire of maternal behaviors, the OB has already been identified as a potential locus of change. A large body of work was performed with sheep and focused mainly on the neurochemical changes in the OB following parturition. Those studies revealed that parturition and exposure to the newborn ewes modulates OB levels of nitric oxide, oxytocin, aspartate, noradrenaline, acetylcholine, GABA, and even glutamate (Kendrick et al., 1988, 1992, 1997). Noradrenaline has also been shown to be necessary for maternal plasticity in mice (Dickinson and Keverne, 1988). The effect of these changes on functional output for different odors and odor coding in general remained largely unexplored, particularly at the population level. We show that changes in mothers are 2-fold. On one hand, there is general dominance of inhibition that sparsens MC representations of simple monomolecular odors. On the other hand, odors that are behaviorally relevant are spared from this general reduction of odor-evoked activity. How can these two phenomena occur simultaneously?

We tested two hypotheses to explain these different effects. First, we examined the hypothesis that inhibitory activity will behave differently at different concentrations in mothers and naive females. For example, inhibition could be driven non-linearly in mothers. Our results argue against this idea (Figure 5). Second, mixture suppression is a well-known phenomenon in olfactory processing that is probably mediated by inhibition (Shen et al., 2013; Davison and Katz, 2007; Giraudet et al., 2002; Olsen et al., 2010). Thus, we examined whether the differential response to natural odors in mothers is the result of a basic difference in processing of mixtures versus pure odors. This idea was also ruled out (Figure 4). One alternative explanation we favor is that there may be specific changes in particular OB regions encoding behaviorally relevant odors. Future studies are needed to identify the loci of differential changes and the cellular factors that regulate which MCs are affected and which are spared.

Differential Plasticity of Behaviorally Relevant Odors

Different odors are routed into the OB through different functional channels that are spatially segregated (Buck and Axel, 1991; Mombaerts, 2006). This anatomical and molecular segregation allows, at least potentially, a simple way to regulate specific channels by virtue of local mechanisms. In the OB, each receptor is activated by several odors. Thus, the plasticity of specific ''sensory channels'' is expected to change specific regions of the receptive range of MCs. This is supported by our analysis of neurons responding to both natural and pure odors within their receptive range.

The literature on plastic changes in the main OB is diverse. There is evidence that plasticity induces odor-specific changes

(C) Ten MCs and their maximum response to all 11 odors presented (pure + natural) from the same recorded field. Top, naive female; bottom, mother.
(D) Pairwise correlation matrices from the representative MCs in (C).
(E) Mean pairwise correlation for all odors together, all odors shuffled, only pure odors, and only natural odors, respectively. ***$p < 0.0001$, Mann-Whitney *U* test. For each box, the central mark indicates the median and the bottom and top edges indicate the 25th and 75th percentiles, respectively. The whiskers extend to the most extreme data points.
(F) Diagrammatic representation of how population response profiles were analyzed. For simplification, a network comprised of only 2 neurons is shown (all neurons were used for each odor response vector in our analysis). Each response to a given odor (here, a, b, c, etc.) was plotted as a vector of the calcium response magnitude of all responsive neurons (neuron 1, neuron 2, etc.). When the vector for a given odor was constructed, the Euclidean distance (d, top) and cosine similarity (cos, bottom) between all pairs of vectors was calculated (here, cos/d(a,b), cos/d(a,c), and cos/d(b,c) are shown in gray).
(G) Each matrix shows all pairwise distances between all odors in both groups (mothers, n = 78 pairs from 4 mice; naive females, n = 78 pairs from 4 mice). Dotted lines denote the pairwise comparisons restricted to pure odors (blue dotted line) and those restricted to natural odors (magenta dotted line). Top: Euclidean distance; bottom, cosine similarity. Odors: butanal (but), pentanal (pent), ethyl tiglate (e-tig), propanal (prop), methyl propionate (m-prop), ethyl butyrate (e-but), male urine (Um), female urine (Uf), peanut butter (PB), TMT, nest bedding + pup (nest).
(H) The pairwise similarities and pairwise distances among pure odors are not significantly different between naive females and mothers (Wilcoxon rank-sum test; distance, $p = 0.8$; similarity, $p = 0.11$). The pairwise similarities and distances among natural odors are significantly higher in mothers compared with naive females (Wilcoxon rank-sum test; distance, **$p = 2.4e{-}04$; similarity, *$p = 0.038$).
(I) Principal-component analysis (PCA) showing the three first PCAs for all odors (n = 11 odors + blank) and all trials (n = 4) pooled across MCs of all animals per group. Left, naive females; right, mothers.

in MC responses. However, there is also evidence showing global effects, including inhibition (Kato et al., 2012; Buonviso and Chaput, 2000; Chaudhury et al., 2010; Fletcher and Wilson, 2003; Wilson, 2000). Our data here favor a unique scenario in mothers, showing a combined phenotype. We show a global (non-odor-specific) decrease in MC activity, likely due to, in part, increased inhibition (Figures 1, 2, and 6; Figures S2 and S4).

Although we found strong evidence for enhanced inhibition in the MOB of mothers, we note that this is not the only possible mechanism for sparsening and/or reduced responses in MCs. Other possibilities include loss of sensitivity at the level of receptor activation (Dey et al., 2015), changes in the strength of synaptic input to postsynaptic neurons (Tyler et al., 2007), and/or changes in the intrinsic properties of MCs, as recently seen in the accessory olfactory system (Gao et al., 2017). Alternatively, MC plasticity may be mediated by changes in cortical feedback, which largely targets local interneuron populations (Boyd et al., 2012; Markopoulos et al., 2012). Interestingly, subpopulations of cells in the piriform cortex selectively express oxytocin receptors that link them to processing of biologically relevant social odor cues (Choe et al., 2015). Any of these mechanisms could potentially operate in parallel to enhance local circuit inhibition in the OB.

Population Coding in the OB of Mothers

We observe sparser representation of general odors in mothers. What might be the implications of the sparsening to odor coding? Computational and theoretical studies have highlighted the potential advantages of sparse coding for efficient representation of stimuli in several sensory systems (Barth and Poulet, 2012; Brecht and Sakmann, 2002; DeWeese and Zador, 2006; Froudarakis et al., 2014; Hromádka et al., 2008; Miura et al., 2012; Vinje and Gallant, 2000). Sparse coding has been suggested to reduce the overlap between stimulus representations, thus limiting interference and facilitating accurate comparisons between stimulus-evoked patterns and stored memories (Barlow, 1961; Olshausen and Field, 2004; Simoncelli and Olshausen, 2001; but see Spanne and Jörntell, 2015). Recent studies highlight the computational advantage of sparser coding and heightened inhibition in the OB (Abraham et al., 2010; Kato et al., 2012). A natural interpretation of our data could therefore be that sparsening by increased inhibition is advantageous to odor discrimination. Our population analysis reveals a different picture in the OB of mothers. Sparsening did not improve coding of pure odors, which were separated to begin with. However, strengthening of the weak responses to the natural odors improved the separation (Figure 7). One possibility to explore in future studies is whether the general reduced MC activation increases the comparative salience of the behaviorally relevant odors.

Inhibitory Mechanisms of Plasticity in the OB

There are several different types of GABAergic interneurons in the OB that could contribute to increased inhibition in mothers (Aungst et al., 2003; Batista-Brito et al., 2008; Kosaka and Kosaka, 2011). The increase in global inhibition could have been mediated via inhibitory neurons such as dopaminergic periglomerular cells and external plexiform layer interneurons, which are known to have global effects (Huang et al., 2013; Uchida et al., 2014; Kato et al., 2013; Banerjee et al., 2015). However, our concentration experiment (Figure 5) argues that the mechanisms responsible for gain control seems to stay intact after parturition and are less likely to be the suspect of the effects we describe.

The selective effects on behaviorally relevant odors are more likely mediated via neurons that project locally, like periglomerular neurons (PGNs) and granule cells (GCs) (Murthy, 2011a; Wilson and Mainen, 2006). The GC population is a particularly good candidate in this regard. GCs, the largest interneuron population in the OB, serve as an inhibitory feedback module driven by MCs themselves. Surprisingly, only small effects were found on MC inhibition when silencing large cohorts of these interneurons with optogenetics (Fukunaga et al., 2014). However, other findings attributed strong effects of GC inhibition to MC activity and highlighted their importance in MC decorrelation and odor discrimination (Gschwend et al., 2015). Although we still know little about the role of GCs in vivo, they seem to be perfectly situated for fine-tuning specific pathways because they are continuously replaced (Adam and Mizrahi, 2011; Sailor et al., 2016; Lledo et al., 2006). Indeed, selective plasticity by adult-born neurons was recently shown for associative learning paradigms (Geramita et al., 2016; Huang et al., 2016). Moreover, pregnancy drives elevated influx of inhibitory adult-born GCs, which is followed by enhanced integration of these cells into the network during motherhood (Kopel et al., 2012; Shingo et al., 2003; Sakamoto et al., 2011).

Last, we note that other mechanisms may well play a role in the changes accompanying the transition to motherhood. These include, but are not limited to, changes in feedforward inputs to the MCs by olfactory sensory neurons as well as feedback connectivity from higher brain centers or neuromodulatory centers. Although our data suggest that the OB in mothers operates in a different physiological state, the underlying mechanisms are most likely numerous. Cooperative activity of several sources, both local and global, will mediate the increased global inhibition and local excitation reported here.

EXPERIMENTAL PROCEDURES

Animals

For calcium imaging of MCs and RNA extraction, we used Thy1-GCaMP3 (Chen et al., 2012) female mice (10–16 weeks old). Mice were obtained from The Jackson Laboratory and maintained at the Hebrew University specific pathogen-free facility. Animal care and experiments were approved by the Hebrew University Animal Care and Use Committee.

Surgical Procedures

We anesthetized mice with an intraperitoneal injection of ketamine and medetomidine (100 mg/kg and 0.83 mg/kg, respectively) and a subcutaneous injection of carprofen (0.004 mg/g). Additionally, we injected mice subcutaneously with dextrose-saline to prevent dehydration. We assessed the depth of anesthesia by monitoring the pinch withdrawal reflex and added ketamine/medetomidine to maintain it. We continuously monitored the animal's rectal temperature and maintained it at 36°C ± 1°C.

For calcium imaging, we made a small incision in the animal's skin and glued a custom-made metal bar to the skull using dental cement. We used this bar to connect the animal to a custom-made stage to allow precise positioning of the animal's head under the microscope for imaging. Next, we performed a craniotomy (2 × 1 mm) over the OB of one hemisphere. We placed 2% low-melting agar (type IIIa, Sigma-Aldrich, St. Louis, MO)

over the craniotomy, covered by a glass coverslip that was then secured with dental cement.

For MC imaging in awake mice, we used chronic window implantation. For chronic window implantation, a craniotomy was opened over the OBs of both hemispheres. The exposed brain was covered directly with a 3 × 2 mm square glass (Menzel-Glaser, 22 × 22 mm, #3). The margin between the coverglass and the intact bone was gently sealed with Histoacryl glue (B. Braun). After surgery, mice were treated with carprofen (0.004 mg/g, subcutaneously [s.c.]) until full recovery. All animals were allowed to fully recover before the first imaging session, which started at least 2 weeks after surgery.

Two-Photon Calcium Imaging

We performed calcium imaging of the OB using an Ultima two-photon microscope from Prairie Technologies (Middleton, WI), equipped with a 16× water immersion objective lens (0.8 numerical aperture [NA], CF175, Nikon, Tokyo, Japan). We delivered two-photon excitation at 950 nm using a DeepSee femtosecond laser (Spectra Physics, Santa Clara, CA). We extended the laser beam to fill the large back aperture of the 16× objective with an acquisition rate of ~7 Hz. For awake imaging, 2 weeks after window implantation, mice with detectable MCs were habituated under the microscope in a head-fixed position (once a day, 15 min, 4 days). Awake imaging was performed in habituated mice that showed no obvious sign of stress. For time-lapse imaging, 1 day after the first imaging session, a male was introduced for 1 week. After 2 weeks and before parturition, females were isolated.

Data Analysis

We analyzed the data using ImageJ, followed by a custom code written in MATLAB (MathWorks). We manually drew regions of interest (ROIs) corresponding to individual cell bodies and used ImageJ to extract the mean fluorescence of each cell body used for analysis. Because we triggered odor delivery at the onset of inhalation, we aligned all trials according to the frame imaged at odor onset. We calculated relative ΔF/F using the mean fluorescence over 1 s before odor onset as the baseline fluorescence (F0). We low pass-filtered the traces using a square filter with a 3-sample window and phase-filtering by two passes of the filter using the MATLAB filtfilt function. We defined a response window equal to the stimulus duration + 4 s (6- or 19-s window). We categorized calcium transients as odor-evoked responses when at least 2 trials in addition to the mean trace met the following conditions: 3 consecutive ΔF/F values within the response window were found to be above the mean +1.6 SD (4 SD in awake mice) of the values in the 2 s preceding odor onset and the peak ΔF/F amplitude was higher than the ΔF/F amplitude of the blank trial (1.5 times higher in awake mice). Response magnitude was defined as the peak ΔF/F along the response window, averaged between all trials. Distribution values of the area under the receiving operating characteristic (ROC) curve yielded values of 0.96 in anesthetized and 0.94 in awake mouse responses. We defined response onset as the time where 3 consecutive ΔF/F values reached 20% of the maximum response value. For statistical tests on calcium imaging responses, we used non-parametric tests and Kolmogorov-Smirnov test on the cumulative data. Multiple testing was corrected with Bonferroni correction, and, when appropriate, the data are presented and analyzed per animal.

Additional procedures on immunohistochemistry and microscopy, data analysis, respiration-triggered odor delivery, RNA extraction, cDNA preparation, qPCR, and slice electrophysiology can be found in the Supplemental Experimental Procedures.

SUPPLEMENTAL INFORMATION

Supplemental Information includes Supplemental Experimental Procedures, four figures, and one table and can be found with this article online at https://doi.org/10.1016/j.celrep.2017.09.038.

AUTHOR CONTRIBUTIONS

Y.F.S., A.V., and A.M. conceived the project and designed the experiments. A.V. and Y.F.S. carried out and analyzed the imaging experiments. Y.G. and I.D. carried out and analyzed the slice electrophysiology experiment. D.M. and A.C. carried out and analyzed the RNA expression experiment. M.S. carried out additional data analyses. Y.F.S., A.V., and A.M. wrote the paper.

ACKNOWLEDGMENTS

We thank the members of the Mizrahi laboratory, Liqun Luo, Lior Cohen, Ran Darshan, and Yoram Burak for comments and discussions on early versions of this manuscript. This work was supported by a consolidator grant from the European Research Council (616063 to A.M.), the Gatsby Charitable Foundation, the Max Planck Hebrew University Center for Sensory Processing of the Brain in Action, the I-CORE Program of the Planning and Budgeting Committee (#1796/12), and Israel Science Foundation Grant 393/12 (to A.C.).

Received: October 19, 2016
Revised: June 21, 2017
Accepted: September 11, 2017
Published: October 10, 2017

REFERENCES

Abraham, N.M., Egger, V., Shimshek, D.R., Renden, R., Fukunaga, I., Sprengel, R., Seeburg, P.H., Klugmann, M., Margrie, T.W., Schaefer, A.T., and Kuner, T. (2010). Synaptic inhibition in the olfactory bulb accelerates odor discrimination in mice. Neuron *65*, 399–411.

Adam, Y., and Mizrahi, A. (2011). Long-term imaging reveals dynamic changes in the neuronal composition of the glomerular layer. J. Neurosci. *31*, 7967–7973.

Adam, Y., Livneh, Y., Miyamichi, K., Groysman, M., Luo, L., and Mizrahi, A. (2014). Functional transformations of odor inputs in the mouse olfactory bulb. Front. Neural Circuits *8*, 129.

Akerboom, J., Chen, T.W., Wardill, T.J., Tian, L., Marvin, J.S., Mutlu, S., Calderón, N.C., Esposti, F., Borghuis, B.G., Sun, X.R., et al. (2012). Optimization of a GCaMP calcium indicator for neural activity imaging. J. Neurosci. *32*, 13819–13840.

Aungst, J.L., Heyward, P.M., Puche, A.C., Karnup, S.V., Hayar, A., Szabo, G., and Shipley, M.T. (2003). Centre-surround inhibition among olfactory bulb glomeruli. Nature *426*, 623–629.

Banerjee, A., Marbach, F., Anselmi, F., Koh, M.S., Davis, M.B., Garcia da Silva, P., Delevich, K., Oyibo, H.K., Gupta, P., Li, B., and Albeanu, D.F. (2015). An Interglomerular Circuit Gates Glomerular Output and Implements Gain Control in the Mouse Olfactory Bulb. Neuron *87*, 193–207.

Barlow, H.B. (1961). Possible principles underlying the transformations of sensory messages. In Sensory Communication, W.A. Rosenblith, ed. (MIT Press).

Barth, A.L., and Poulet, J.F. (2012). Experimental evidence for sparse firing in the neocortex. Trends Neurosci. *35*, 345–355.

Batista-Brito, R., Close, J., Machold, R., and Fishell, G. (2008). The distinct temporal origins of olfactory bulb interneuron subtypes. J. Neurosci. *28*, 3966–3975.

Boyd, A.M., Sturgill, J.F., Poo, C., and Isaacson, J.S. (2012). Cortical feedback control of olfactory bulb circuits. Neuron *76*, 1161–1174.

Brecht, M., and Sakmann, B. (2002). Dynamic representation of whisker deflection by synaptic potentials in spiny stellate and pyramidal cells in the barrels and septa of layer 4 rat somatosensory cortex. J. Physiol. *543*, 49–70.

Buck, L., and Axel, R. (1991). A novel multigene family may encode odorant receptors: a molecular basis for odor recognition. Cell *65*, 175–187.

Buonviso, N., and Chaput, M. (2000). Olfactory experience decreases responsiveness of the olfactory bulb in the adult rat. Neuroscience *95*, 325–332.

Carlson, G.C., Shipley, M.T., and Keller, A. (2000). Long-lasting depolarizations in mitral cells of the rat olfactory bulb. J. Neurosci. *20*, 2011–2021.

Chaudhury, D., Manella, L., Arellanos, A., Escanilla, O., Cleland, T.A., and Linster, C. (2010). Olfactory bulb habituation to odor stimuli. Behav. Neurosci. *124*, 490–499.

Chen, Q., Cichon, J., Wang, W., Qiu, L., Lee, S.J., Campbell, N.R., Destefino, N., Goard, M.J., Fu, Z., Yasuda, R., et al. (2012). Imaging neural activity using Thy1-GCaMP transgenic mice. Neuron *76*, 297–308.

Choe, H.K., Reed, M.D., Benavidez, N., Montgomery, D., Soares, N., Yim, Y.S., and Choi, G.B. (2015). Oxytocin Mediates Entrainment of Sensory Stimuli to Social Cues of Opposing Valence. Neuron *87*, 152–163.

Chu, M.W., Li, W.L., and Komiyama, T. (2016). Balancing the Robustness and Efficiency of Odor Representations during Learning. Neuron *92*, 174–186.

Davison, I.G., and Katz, L.C. (2007). Sparse and selective odor coding by mitral/tufted neurons in the main olfactory bulb. J. Neurosci. *27*, 2091–2101.

DeWeese, M.R., and Zador, A.M. (2006). Non-Gaussian membrane potential dynamics imply sparse, synchronous activity in auditory cortex. J. Neurosci. *26*, 12206–12218.

Dey, S., Chamero, P., Pru, J.K., Chien, M.S., Ibarra-Soria, X., Spencer, K.R., Logan, D.W., Matsunami, H., Peluso, J.J., and Stowers, L. (2015). Cyclic Regulation of Sensory Perception by a Female Hormone Alters Behavior. Cell *161*, 1334–1344.

Dickinson, C., and Keverne, E.B. (1988). Importance of noradrenergic mechanisms in the olfactory bulbs for the maternal behaviour of mice. Physiol. Behav. *43*, 313–316.

Dulac, C., O'Connell, L.A., and Wu, Z. (2014). Neural control of maternal and paternal behaviors. Science *345*, 765–770.

Elyada, Y.M., and Mizrahi, A. (2015). Becoming a mother-circuit plasticity underlying maternal behavior. Curr. Opin. Neurobiol. *35*, 49–56.

Fletcher, M.L., and Wilson, D.A. (2003). Olfactory bulb mitral-tufted cell plasticity: odorant-specific tuning reflects previous odorant exposure. J. Neurosci. *23*, 6946–6955.

Froudarakis, E., Berens, P., Ecker, A.S., Cotton, R.J., Sinz, F.H., Yatsenko, D., Saggau, P., Bethge, M., and Tolias, A.S. (2014). Population code in mouse V1 facilitates readout of natural scenes through increased sparseness. Nat. Neurosci. *17*, 851–857.

Fukunaga, I., Herb, J.T., Kollo, M., Boyden, E.S., and Schaefer, A.T. (2014). Independent control of gamma and theta activity by distinct interneuron networks in the olfactory bulb. Nat. Neurosci. *17*, 1208–1216.

Gao, Y., Budlong, C., Durlacher, E., and Davison, I.G. (2017). Neural mechanisms of social learning in the female mouse. eLife *6*.

Geramita, M.A., Burton, S.D., and Urban, N.N. (2016). Distinct lateral inhibitory circuits drive parallel processing of sensory information in the mammalian olfactory bulb. eLife *5*.

Giraudet, P., Berthommier, F., and Chaput, M. (2002). Mitral cell temporal response patterns evoked by odor mixtures in the rat olfactory bulb. J. Neurophysiol. *88*, 829–838.

Gire, D.H., Franks, K.M., Zak, J.D., Tanaka, K.F., Whitesell, J.D., Mulligan, A.A., Hen, R., and Schoppa, N.E. (2012). Mitral cells in the olfactory bulb are mainly excited through a multistep signaling path. J. Neurosci. *32*, 2964–2975.

Gschwend, O., Abraham, N.M., Lagier, S., Begnaud, F., Rodriguez, I., and Carleton, A. (2015). Neuronal pattern separation in the olfactory bulb improves odor discrimination learning. Nat. Neurosci. *18*, 1474–1482.

Hromádka, T., Deweese, M.R., and Zador, A.M. (2008). Sparse representation of sounds in the unanesthetized auditory cortex. PLoS Biol. *6*, e16.

Huang, L., Garcia, I., Jen, H.I., and Arenkiel, B.R. (2013). Reciprocal connectivity between mitral cells and external plexiform layer interneurons in the mouse olfactory bulb. Front. Neural Circuits *7*, 32.

Huang, L., Ung, K., Garcia, I., Quast, K.B., Cordiner, K., Saggau, P., and Arenkiel, B.R. (2016). Task Learning Promotes Plasticity of Interneuron Connectivity Maps in the Olfactory Bulb. J. Neurosci. *36*, 8856–8871.

Kato, H.K., Chu, M.W., Isaacson, J.S., and Komiyama, T. (2012). Dynamic sensory representations in the olfactory bulb: modulation by wakefulness and experience. Neuron *76*, 962–975.

Kato, H.K., Gillet, S.N., Peters, A.J., Isaacson, J.S., and Komiyama, T. (2013). Parvalbumin-expressing interneurons linearly control olfactory bulb output. Neuron *80*, 1218–1231.

Kendrick, K.M., Keverne, E.B., Chapman, C., and Baldwin, B.A. (1988). Microdialysis measurement of oxytocin, aspartate, γ-aminobutyric acid and glutamate release from the olfactory bulb of the sheep during vaginocervical stimulation. Brain Res. *442*, 171–174.

Kendrick, K.M., Lévy, F., and Keverne, E.B. (1992). Changes in the sensory processing of olfactory signals induced by birth in sheep. Science *256*, 833–836.

Kendrick, K.M., Guevara-Guzman, R., Zorrilla, J., Hinton, M.R., Broad, K.D., Mimmack, M., and Ohkura, S. (1997). Formation of olfactory memories mediated by nitric oxide. Nature *388*, 670–674.

Kobayakawa, K., Kobayakawa, R., Matsumoto, H., Oka, Y., Imai, T., Ikawa, M., Okabe, M., Ikeda, T., Itohara, S., Kikusui, T., et al. (2007). Innate versus learned odour processing in the mouse olfactory bulb. Nature *450*, 503–508.

Kopel, H., Schechtman, E., Groysman, M., and Mizrahi, A. (2012). Enhanced synaptic integration of adult-born neurons in the olfactory bulb of lactating mothers. J. Neurosci. *32*, 7519–7527.

Kosaka, T., and Kosaka, K. (2011). "Interneurons" in the olfactory bulb revisited. Neurosci. Res. *69*, 93–99.

Lévy, F., and Keller, M. (2009). Olfactory mediation of maternal behavior in selected mammalian species. Behav. Brain Res. *200*, 336–345.

Lévy, F., Gervais, R., Kindermann, U., Orgeur, P., and Piketty, V. (1990). Importance of beta-noradrenergic receptors in the olfactory bulb of sheep for recognition of lambs. Behav. Neurosci. *104*, 464–469.

Livneh, Y., Adam, Y., and Mizrahi, A. (2014). Odor processing by adult-born neurons. Neuron *81*, 1097–1110.

Lledo, P.M., Alonso, M., and Grubb, M.S. (2006). Adult neurogenesis and functional plasticity in neuronal circuits. Nat. Rev. Neurosci. *7*, 179–193.

Markopoulos, F., Rokni, D., Gire, D.H., and Murthy, V.N. (2012). Functional properties of cortical feedback projections to the olfactory bulb. Neuron *76*, 1175–1188.

Miura, K., Mainen, Z.F., and Uchida, N. (2012). Odor representations in olfactory cortex: distributed rate coding and decorrelated population activity. Neuron *74*, 1087–1098.

Mombaerts, P. (2006). Axonal wiring in the mouse olfactory system. Annu. Rev. Cell Dev. Biol. *22*, 713–737.

Murthy, V.N. (2011a). Olfactory maps in the brain. Annu. Rev. Neurosci. *34*, 233–258.

Numan, M. (2006). Hypothalamic neural circuits regulating maternal responsiveness toward infants. Behav. Cogn. Neurosci. Rev. *5*, 163–190.

Olsen, S.R., Bhandawat, V., and Wilson, R.I. (2010). Divisive normalization in olfactory population codes. Neuron *66*, 287–299.

Olshausen, B.A., and Field, D.J. (2004). Sparse coding of sensory inputs. Curr. Opin. Neurobiol. *14*, 481–487.

Poindron, P. (2005). Mechanisms of activation of maternal behaviour in mammals. Reprod. Nutr. Dev. *45*, 341–351.

Rinberg, D., Koulakov, A., and Gelperin, A. (2006). Sparse odor coding in awake behaving mice. J. Neurosci. *26*, 8857–8865.

Root, C.M., Denny, C.A., Hen, R., and Axel, R. (2014). The participation of cortical amygdala in innate, odour-driven behaviour. Nature *515*, 269–273.

Sailor, K.A., Valley, M.T., Wiechert, M.T., Riecke, H., Sun, G.J., Adams, W., Dennis, J.C., Sharafi, S., Ming, G.L., Song, H., and Lledo, P.M. (2016). Persistent Structural Plasticity Optimizes Sensory Information Processing in the Olfactory Bulb. Neuron *91*, 384–396.

Sakamoto, M., Imayoshi, I., Ohtsuka, T., Yamaguchi, M., Mori, K., and Kageyama, R. (2011). Continuous neurogenesis in the adult forebrain is required for innate olfactory responses. Proc. Natl. Acad. Sci. USA *108*, 8479–8484.

Schaefer, A.T., and Margrie, T.W. (2007). Spatiotemporal representations in the olfactory system. Trends Neurosci. *30*, 92–100.

Shen, K., Tootoonian, S., and Laurent, G. (2013). Encoding of mixtures in a simple olfactory system. Neuron *80*, 1246–1262.

Shingo, T., Gregg, C., Enwere, E., Fujikawa, H., Hassam, R., Geary, C., Cross, J.C., and Weiss, S. (2003). Pregnancy-stimulated neurogenesis in the adult female forebrain mediated by prolactin. Science *299*, 117–120.

Simoncelli, E.P., and Olshausen, B.A. (2001). Natural image statistics and neural representation. Annu. Rev. Neurosci. *24*, 1193–1216.

Spanne, A., and Jörntell, H. (2015). Questioning the role of sparse coding in the brain. Trends Neurosci. *38*, 417–427.

Tian, L., Hires, S.A., Mao, T., Huber, D., Chiappe, M.E., Chalasani, S.H., Petreanu, L., Akerboom, J., McKinney, S.A., Schreiter, E.R., et al. (2009). Imaging neural activity in worms, flies and mice with improved GCaMP calcium indicators. Nat. Methods *6*, 875–881.

Tyler, W.J., Petzold, G.C., Pal, S.K., and Murthy, V.N. (2007). Experience-dependent modification of primary sensory synapses in the mammalian olfactory bulb. J. Neurosci. *27*, 9427–9438.

Uchida, N., Poo, C., and Haddad, R. (2014). Coding and transformations in the olfactory system. Annu. Rev. Neurosci. *37*, 363–385.

Vinje, W.E., and Gallant, J.L. (2000). Sparse coding and decorrelation in primary visual cortex during natural vision. Science *287*, 1273–1276.

Wachowiak, M., Economo, M.N., Díaz-Quesada, M., Brunert, D., Wesson, D.W., White, J.A., and Rothermel, M. (2013). Optical dissection of odor information processing in vivo using GCaMPs expressed in specified cell types of the olfactory bulb. J. Neurosci. *33*, 5285–5300.

Wilson, D.A. (2000). Comparison of odor receptive field plasticity in the rat olfactory bulb and anterior piriform cortex. J. Neurophysiol. *84*, 3036–3042.

Wilson, R.I., and Mainen, Z.F. (2006). Early events in olfactory processing. Annu. Rev. Neurosci. *29*, 163–201.

Wu, Z., Autry, A.E., Bergan, J.F., Watabe-Uchida, M., and Dulac, C.G. (2014). Galanin neurons in the medial preoptic area govern parental behaviour. Nature *509*, 325–330.

Zilkha, N., Scott, N., and Kimchi, T. (2017). Sexual Dimorphism of Parental Care: From Genes to Behavior. Annu. Rev. Neurosci. *40*, 273–305.

Cell Reports, Volume *21*

Supplemental Information

Functional Plasticity of Odor Representations during Motherhood

Amit Vinograd, Yael Fuchs-Shlomai, Merav Stern, Diptendu Mukherjee, Yuan Gao, Ami Citri, Ian Davison, and Adi Mizrahi

Supplemental experimental procedures

Immunohistochemistry and confocal microscopy For visualization of MCs in confocal microscopy (Fig. 1A), we perfused mice transcardially with PBS, followed by 4% paraformaldehyde and cryoprotected the brain in 30% sucrose overnight. We sectioned OBs coronally on a sliding microtome (40 µm slices), washed the slices in PBS and then incubated them for 2 hours in a blocking solution (5% normal goat serum and 0.4% Triton-X). We incubated slices overnight at room temperature with primary antibodies diluted in the blocking solution (rabbit anti-GFP, Millipore 1:1000) washed them in PBS, and then incubated them for 2 hrs at room temperature with secondary antibodies (Jackson ImmunoResearch), diluted 1:500 in the blocking solution (DyLight488-conjugated goat anti-rabbit). Prior to mounting on microscope slides, we incubated the slices with DAPI (Santa Cruz Biotechnology; 50µg/ml) for 5 min and then washed them with PBS. We obtained confocal images using a Leica SP-5 confocal microscope, using a 40X (1.3 NA) oil objective.

Data analysis Change index (Fig. S1B, S1D, S1F, S1H) was calculated as follows: $\frac{\sum_{n=1}^{number\ of\ odors}(\frac{Mother_n}{Naive_n}-1)}{number\ of\ odors}$ where $Mother_n/Naive_n$ are the values for each odor either for response amplitude (Fig. S1B,S1D) or responsiveness (Fig. S1F, S1H).

For mixture processing analysis (Fig. 4) we calculated the mixture change by subtracting the peak amplitude of the mixture from the strongest activating odor on all responsive cells. Repeating the analysis on all cells, on only responsive to 2 odors and by subtracting the weakest activating odor resulted with qualitatively the same result. For pairwise correlation (Fig. 7E), we calculated the pearson correlation of the maximum ΔF/F in responsive cells between all pairs in each recorded field of the same animal.

The ensemble activity response of MCs to a given odor at each time point was expressed as a vector $\bar{V}_\alpha$, where α denotes the odor and each component i of the vector is the activity of cell i in response to the odor at that time point. Only cells that responded to at

least one odor were included in the ensemble vectors. To evaluate how similar responses to different odors are in cell activities space, we took the response vectors and calculated the cosine similarity between them (see illustrations in Figure 7F):

$$\text{Cosine similarity} = \frac{\sum_{i=1}^{n}(V_{i,\alpha}V_{i,\beta})}{\sqrt{\sum_{i=1}^{n}(V_{i,\alpha})^2}\sqrt{\sum_{i=1}^{n}(V_{i,\beta})^2}}$$

To evaluate how far responses to different odors are in cell activities space, we took the response vectors and calculated the Euclidean distance. We accounted for the different number of cells responding in each population with a normalization factor. The formula is given by:

$$Euclidean\ distance = \frac{1}{\sqrt{n}}\sqrt{\sum_{i=1}^{n}\left(V_{i,\alpha} - V_{i,\beta}\right)^2}$$

with n the number of responding cells (to any odor) which is the number of dimensions contributing to the activity in space. This measure is sensitive to the relative magnitude of the responses and describes the distance in space between them. An intuition to this measure is also given by the separation of the first three principle components of the different odors (Fig. 7I). The visual distances between the principle components of each odor is what is actually measured in Fig. 7G,H with the only exception that instead of using only the first three dimensions (restricted by a plot) we use the full responding cell activities space. Since our main goal was to compare the distribution of separation of odor pairs between mothers and naïve (pure vs. natural) we normalized the resulting distances by dividing all odor pairs in mothers according to the largest odor pair distance received in mothers and the same for all odor pairs in naïve according to the largest odor pair in naïve.

Odor delivery

To deliver odorants we used a custom-made 11 channels olfactometer. In order to avoid cross-contamination between odorants we used separate tubing for each channel, all the

way from the odor vial to the animal's nose. For pure odors we used a panel of 6 odorants known to activate different and partially overlapping areas in the dorsal part of the OB (butanal, pentanal, ethyl-tiglate, propanal, methyl-propionate, ethyl-butyrate and ethyl-acetate; all obtained from Sigma-Aldrich, St. Louis, MO). We presented each pure odorant at a final concentration of 50 ppm, for 2 and 15 seconds with a 15 second inter-stimulus interval, repeated for 4 times, in pseudo-random order. Each repeat included a blank trial consisting of all components of a standard trial, except for odor presentation. For a subset of mice we added to the 6 pure odorants 5 natural odorants- male urine, female urine, peanut butter, trimethylthiazoline (TMT) and nest odor. Urine was collected from thy1-GCaMP3 males and females and stored at -20°c. 10µl was placed in the odor vials. Peanut butter was made of 100% peanuts (Better&different, Mishor Edomim, Israel) and 1gr peanut butter was placed in the vials. For predator odor we used 1µl of TMT (Contech, Delta, Canada). Nest odor was made of 0.5gr nest bedding and 1 pup that was kept warm using a heating pad. For mixtures experiment we used ethyl-acetate methyl-propionate ethyl-tiglate and their mixtures where combined via air in front of the mouse nose. In anesthetized mice, in order to trigger the odor delivery at the onset of inhalation, we monitored the animal's respiration throughout the experiment by a low pressure sensor (1-INCH-D1-4V-MINI, 'All sensors', Morgan Hill, CA). We connected the low pressure sensor to a thin stainless steel tubing (OD 0.7 mm) and placed it at the entrance of the animals' contra-lateral nostril. The information from the pressure sensor was passed to an analogue converter (window discriminator), which we used to identify the inhalation onset during the respiratory cycle. Each odor stimulus was triggered at onset of inhalation.

RNA extraction, cDNA preparation and quantitative PCR

OBs were collected as quickly as possible (normally in less than 2 min) in ice-cold conditions in a clean and RNase free environment, transferred immediately to Tri-Reagent (Sigma) and stored at -80°C until homogenization. Tissue was homogenized using a 25G long needle and RNA was extracted. RNA concentration was determined by a nanodrop spectrophotometer and 300ng of RNA was used for random-primer based

cDNA preparation (Applied Biosystems, High Capacity cDNA Reverse Transcription Kit). cDNA was diluted to 2ng/µl and processed for qPCR analysis using SYBR Green probes in a Light-cycler® 480 Real Time PCR Instrument (Roche Light Cycler*480 SYBR Green I Master). Relative levels of gene expression (ΔCt) were obtained by normalizing gene expression to a housekeeping gene (GAPDH). Fold induction was calculated using the ΔΔCt method, addressing fold induction of OBs from mothers in comparison to OBs from naïve females. Statistical analysis was performed using Excel. Primers were ordered from IDT DNA. A list of primers used and their efficiency is included in supplementary table 1.

Slice electrophysiology

Sagittal brain slices (300 µm thick) were prepared from the main olfactory bulb of lactating mothers C57Bl6/J mice, 3-5 days after parturition (11-14 weeks of age) using a Leica VT1200S vibratome. All animals had litters of ≥3 pups and displayed appropriate maternal care. Control recordings were carried out from group-housed,age-matched females. To obtain viable slices from adult animals, mice were anesthetized with ketamine/xylazine and transcardially perfused with protective artificial cerebrospinal fluid (ACSF) containing, in mM: 124 NaCl, 2.5 KCl, 1.25 NaH_2PO_4, 25 $NaHCO_3$, 75 sucrose, 10 glucose, 1.3 ascorbic acid, 0.5 $CaCl_2$ and 7 $MgCl_2$. Slices were incubated and recorded using standard ACSF containing, in mM: 124 NaCl, 3 KCl, 1.25 NaH_2PO_4, 26 $NaHCO_3$, 20 D-glucose, 2 $CaCl_2$ and 1.5 $MgCl_2$, continuously oxygenated with 95% CO_2 / 5% O_2. Whole cell voltage clamp recordings of mitral cells were carried out at 29.5oC in a submerged recording chamber. Slices were visualized with Dodt contrast using a two-photon imaging system (Prairie Technologies Ultima) and Alexa594 was added to the internal solution to confirm cell type and intact dendritic arbor. For electrical stimulation, glass stimulation pipettes were placed adjacent to the cell's parent glomerulus and the olfactory nerve was stimulated with brief current pulses (0.2ms, 4-12 µA; 120% of threshold). Voltage clamp recordings of miniature synaptic currents were made with high-Cl- internal solutions containing, in mM: 115 CsCl, 25 TEA-Cl, 5 QX314-Cl, 0.2 EGTA, 4 MgATP, 0.3 Na_3GTP and 10 phosphocreatine disodium. Evoked excitatory / inhibitory synaptic currents were recorded with internal solutions

containing, in mM: 130 Cs Methanesulfonate, 4 NaCl, 10 HEPEs, 1 EGTA (pH with CsOH), 4 MgATP, 0.3 Na3GTP, 10 Phosphocreatine disodium, 25 TEA-OH, 5 QX314-Cl. Electrophysiological data were acquired at 10 KHz using a Multiclamp 700B amplifier (Molecular Devices, Sunnyvale, CA), data acquisition board (USB 1221, National Instruments), and custom MATLAB routines (Mathworks, Natick, MA). Inhibitory events were detected and quantified using Igor Pro (WaveMetrics, Lake Oswego, Oregon).

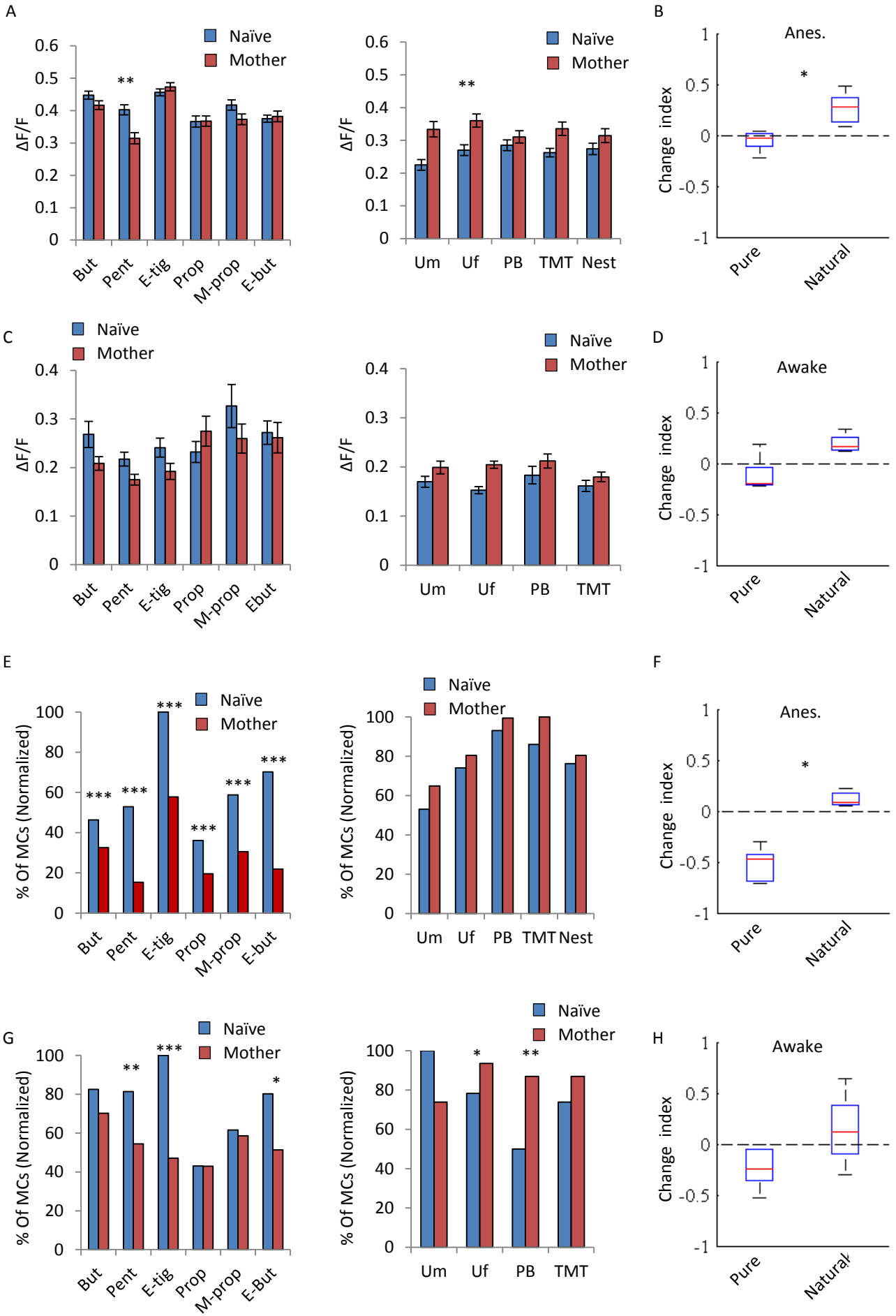
A
Naïve
Mother
ΔF/F
But
Pent
E-tig
Prop
M-prop
E-but
Um
Uf
PB
TMT
Nest
B
Anes.
Change index
Pure
Natural
C
Ebut
D
Awake
E
% Of MCs (Normalized)
F
G
E-But
H

Figure S1

Fig. S1. Analysis per-odor shows increased sparsening to pure odors and higher responsiveness to natural odors, related to Figure 1, 2 and 3. (A) Left - Average ΔF/F response values to the different pure odors in anesthetized Naïve females (blue) and Mothers (red). Black error bars- SEM. Right - same as 'A' for natural odors. **(B)** Change index of average ΔF/F response values between Naïve females and Mothers for pure and natural odors. In each box, red lines represent the median, edges are the 25th and 75th percentiles, top and bottom bars show the most extreme data points. **(C-D)** Same as A-B but for awake mice. **(E)** Left - Percentage of cells responding to each individual pure odor normalized to the most responsive odor. Blue bars- Naïve females, red- Mothers. Right - Same as 'D' but for natural odors. **(E)** Change index of responsiveness values between naïve females and mothers for pure and natural odors. **(G-H)** Same as E-F but for awake mice. (*p<0.05, **p<0.001, ***p<0.0001, A,C-binomial proportion test, B,D,E,F,G,H - Mann-Whitney U test).

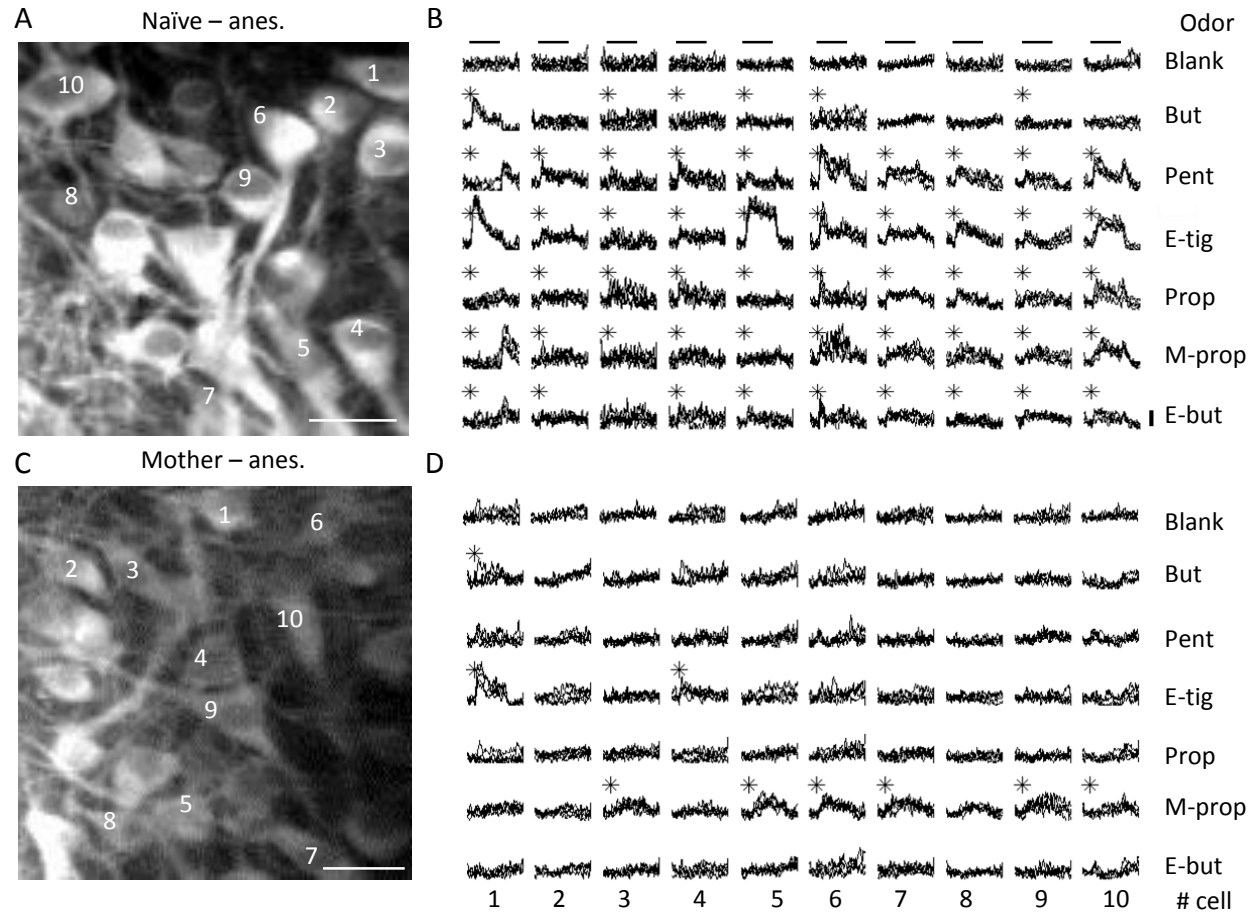
A
Naïve – anes.
10
1
6
2
3
8
9
5
4
7
B
Odor
Blank
But
Pent
E-tig
Prop
M-prop
E-but
C
Mother – anes.
1
6
2
3
10
4
9
8
5
7
D
Blank
But
Pent
E-tig
Prop
M-prop
E-but
1 2 3 4 5 6 7 8 9 10
cell

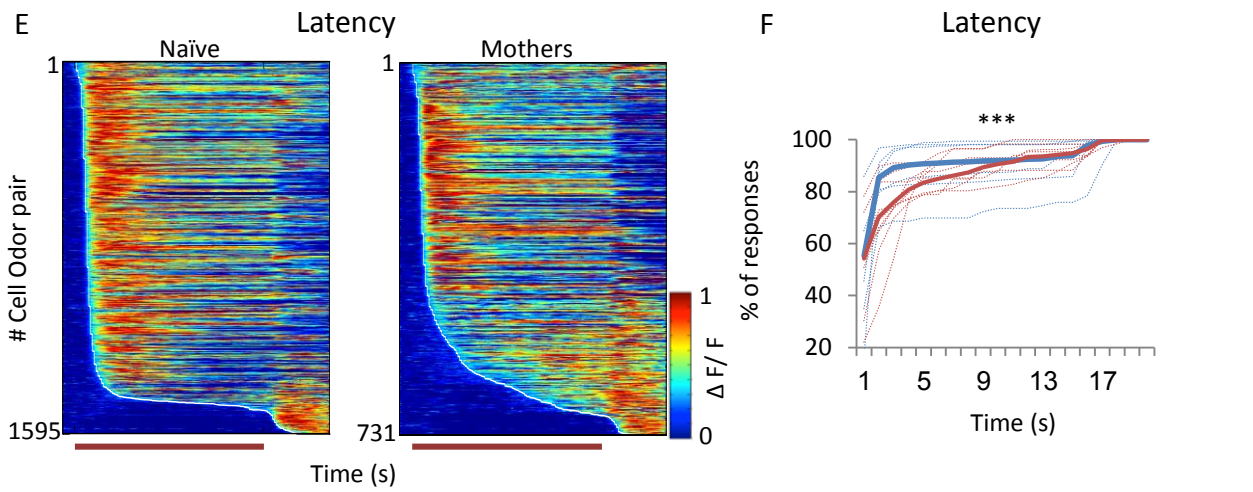
E
Latency
Naïve
Mothers
1
1595
731
Cell Odor pair
Time (s)
1
0
Δ F/ F
F
Latency
***
100
80
60
40
20
% of responses
1 5 9 13 17
Time (s)

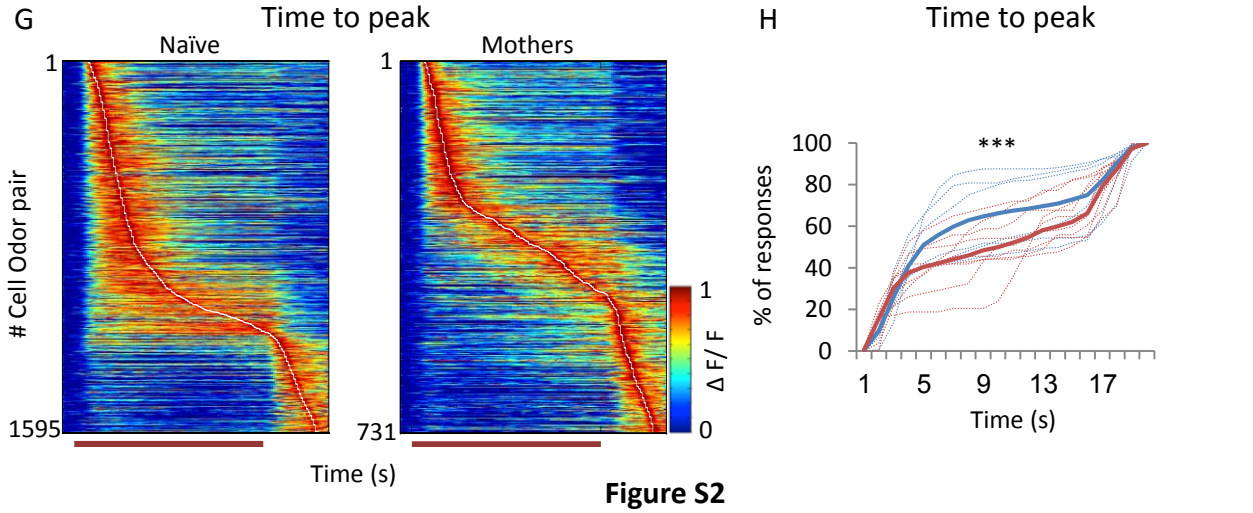
G
Time to peak
Naïve
Mothers
1
1595
731
Cell Odor pair
Time (s)
1
0
Δ F/ F
H
Time to peak
***
100
80
60
40
20
0
% of responses
1 5 9 13 17
Time (s)

Figure S2

- **Fig. S2. Changes in MC responses to persistent odor stimulation in mothers, related to Figure 1. (A)** Two photon micrograph of a representative field used for imaging in a naïve female. Scale bar, 20μm. **(B)** Calcium transients elicited by the neurons in the field shown in A (cells marked by numbers in A) in response to a 15 second odor stimulation with 6 odors. Each line represents a single trial. Black asterisk denotes a statistically significant response. Vertical bar - 25% ΔF/F. **(C-D)** As in 'A-B' but example from a mother. **(E)** Time course for all the responsive cell-odor pairs in naïve females (left panel) and mothers (right panel) normalized to the peak response and sorted by latency to respond. Horizontal line denotes odor stimulation (15 seconds). **(F)** Cumulative distribution of response latency of all the responsive cell-odor pairs in naïve females (blue) and mothers (red) ($p<0.0001$, Kolmogorov-Smirnov test). Each dashed line represents an individual mouse**. (G)** As in 'E' but data sorted by time to peak. **(H)** As in 'F' but for values of time to peak ($p<0.0001$, Kolmogorov-Smirnov test).

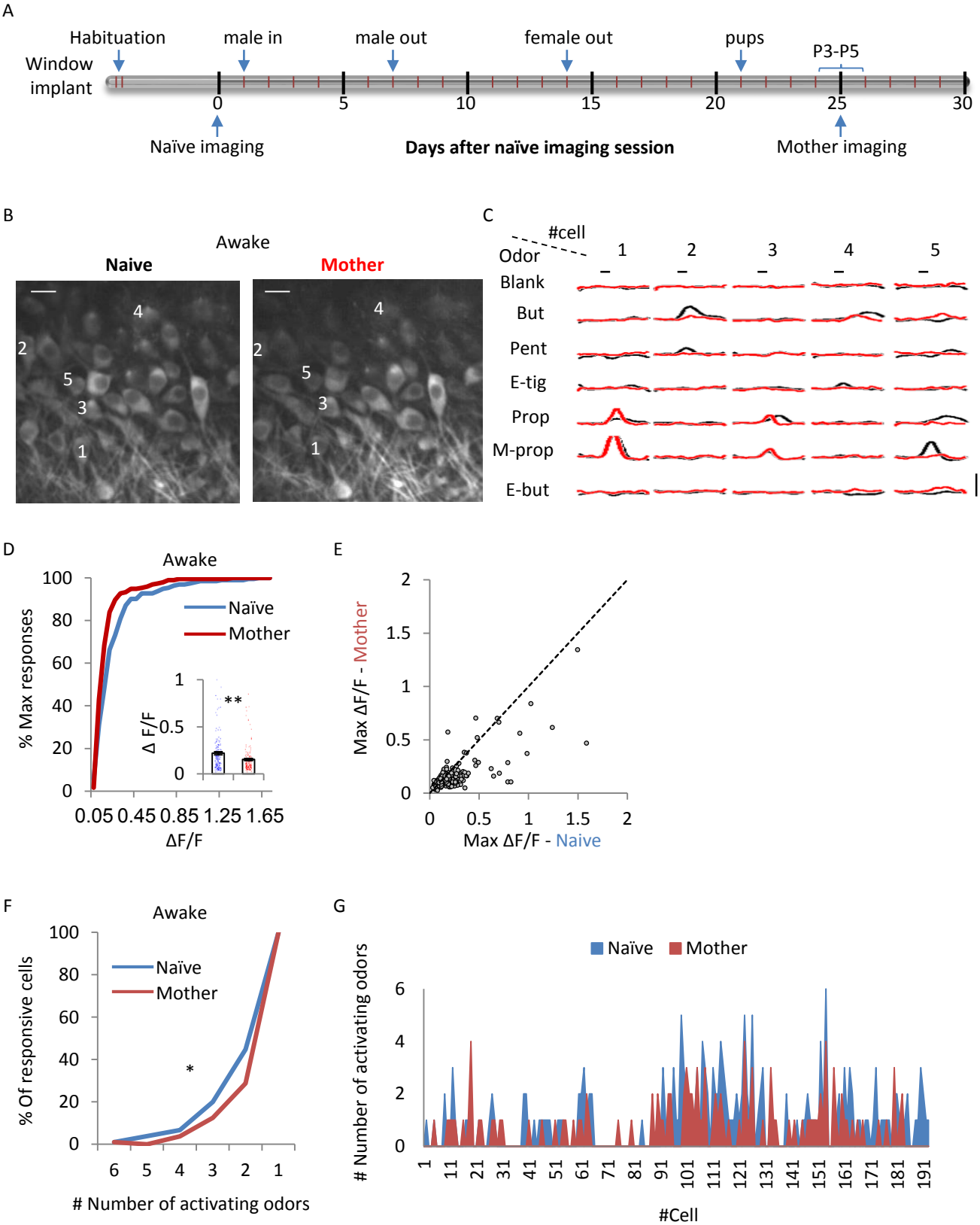
A
Habituation
male in
male out
female out
pups
P3-P5
Window implant
0
5
10
15
20
25
30
Naïve imaging
Days after naïve imaging session
Mother imaging
B
Awake
Naive
Mother
C
#cell
Odor
1
2
3
4
5
Blank
But
Pent
E-tig
Prop
M-prop
E-but
D
Awake
Naïve
Mother
% Max responses
Δ F/F
**
ΔF/F
E
Max ΔF/F - Mother
Max ΔF/F - Naive
F
Awake
Naïve
Mother
% Of responsive cells
*
Number of activating odors
G
Naïve
Mother
Number of activating odors
#Cell

Figure S3

Fig. S3. Time lapse imaging of MCs supports the sparsening of MCs in mothers, related to Figure 2. (A) Experimental timeline. **(B)** Two photon micrograph of a representative field showing the same MCs before (left) and after (right) parturition. Scale bar, 20μm. **(C)** Calcium transients elicited by 5 neurons in the field shown in 'B' in response to a 2 seconds odor stimulation with 6 odors. Each trace represents a mean of 4 trials. Black – naïve females, red - mothers. Vertical bar - 25% ΔF/F. **(D)** Cumulative distribution of peak odor evoked responses before (blue) and after (red) parturition. Inset: Mean±SEM peak amplitude of odor-evoked calcium transients per cell before (blue) and after (red) parturition (**P<0.001, Mann-Whitney U test). **(E)** Max ΔF/F of all individual MCs before (horizontal axis) and after (vertical axis) parturition. **(F)** Cumulative distribution of the percentage of MCs responding to 1-6 odors before (blue) and after (red) parturition (*P<0.01, Kolmogorov-Smirnov test). **(G)** Odor responsiveness in all individual MCs recorded before (blue) and after (red) parturition (n=193 cells).

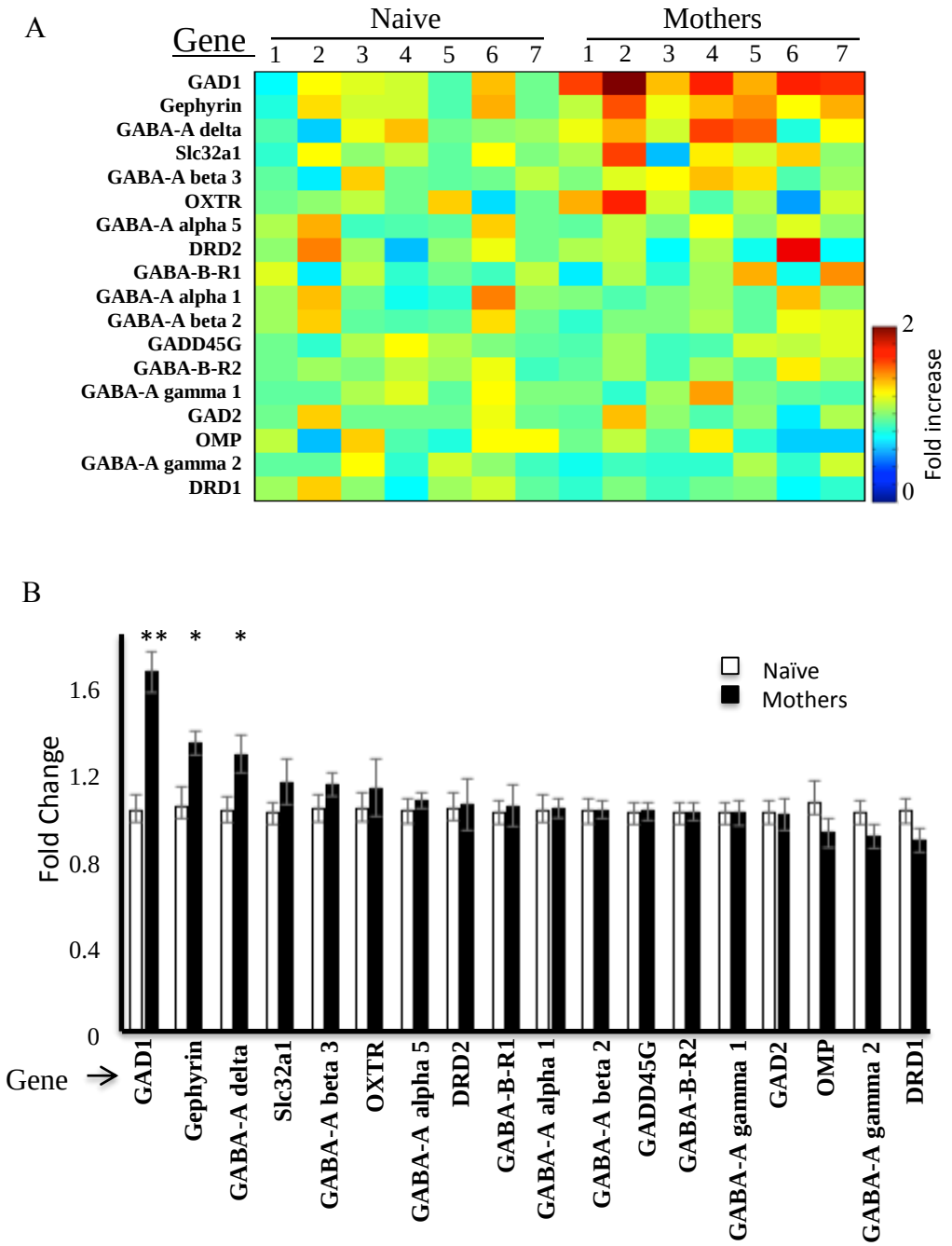
A
Gene
Naive
Mothers
1 2 3 4 5 6 7 1 2 3 4 5 6 7
GAD1
Gephyrin
GABA-A delta
Slc32a1
GABA-A beta 3
OXTR
GABA-A alpha 5
DRD2
GABA-B-R1
GABA-A alpha 1
GABA-A beta 2
GADD45G
GABA-B-R2
GABA-A gamma 1
GAD2
OMP
GABA-A gamma 2
DRD1
2
0
Fold increase
B
Naïve
Mothers
Fold Change
1.6
1.2
0.8
0.4
0
** * *
Gene
GAD1
Gephyrin
GABA-A delta
Slc32a1
GABA-A beta 3
OXTR
GABA-A alpha 5
DRD2
GABA-B-R1
GABA-A alpha 1
GABA-A beta 2
GADD45G
GABA-B-R2
GABA-A gamma 1
GAD2
OMP
GABA-A gamma 2
DRD1

Figure S4

Fig. S4. Increase in GABA signaling pathway genes support increased inhibition in the OB of mothers, related to Figure 6. (A) Heat-map comparing the expression level of genes in individual mice from either Naïve females or Mothers (each pixel is an average of two independently assayed OBs in individual mice). Levels of comparative expression are represented as fold over the average of control. Data is sorted by the level of change in mothers vs naïve (top: highest change). **(B)** Fold induction of the selected genes, comparing average (±SEM) gene expression in the OBs of naïve females and mothers. Statistically significant transcriptional upregulation was observed for GAD67, Gephyrin and GABAA-delta (**p< 0.001 and *p< 0.05, T-test).

Gene name:	Gene abbreviation	Forward Primer	Reverse Primer	% Efficiency
dopamine receptor D1	*Drd1*	acaacggggctgtgatgt	catgagggatcaggtaaacca	102.5
dopamine receptor D2	*Drd2*	tgaacaggcggagaatgg	ctggtgcttgacagcatctc	103.8
gamma-aminobutyric acid type A receptor delta subunit	*Gabrd*	caaggtcaaggtcaccaagc	gggagatagccaactcctga	97.5
gamma-aminobutyric acid type A receptor gamma1 subunit	*Gabrg1*	gaggcaggaagctgaaaaac	tgctgttcatgggaatgaga	101.2
gamma-aminobutyric acid type A receptor gamma2 subunit	*Gabrg2*	ggaatacaactgaagtagtgaagacaa	ttctgctcagatcgaagtacaca	101.6
gamma aminobutyric acid type A receptor alpha1 subunit	*Gabra1*	gcccactaaaattcggaagc	cttctgctacaaccactgaacg	98.1
gamma aminobutyric acid type A receptor alpha5 subunit	*Gabra5*	gacggactcttggatggcta	acctgcgtgattcgctct	99.3
gamma aminobutyric acid type A receptor beta2 subunit	*Gabrb2*	caatatccacgtaggtagagaacact	ttctacatggactgctatttctgg	104.1
gamma aminobutyric acid type A receptor beta3 subunit	*Gabrb3*	ggattgttctcgtaggaataggc	gaaatgaaatcgacgggaatac	108.0
gamma aminobutyric acid type B receptor subunit 1	*Gabbr1*	gctccaagaagatgaatacatgg	ttttggtctcataagcaagaaaga	99.6
gamma aminobutyric acid type B receptor subunit 2	*Gabbr2*	aggtgaaggtcggcgagta	tggtgtcgttgatgatctcc	105.1
gephyrin	*Gphn*	tgatcttcatgctcagatcca	gcaaatgttgttggcaagc	101.7
glutamate decarboxylase 2	*Gad2*	tttccagaagtcaaggagaagg	cagctcccttcttgagagaaaa	102.6
glutamate decarboxylase 1	*Gad1*	tggagatgcgaaccatgag	gaagggttcctggtttagcc	105.8
growth arrest and DNA damage inducible gamma	*Gadd45g*	ggataacttgctgttcgtgga	aagttcgtgcagtgctttcc	102.5
olfactory marker protein	*Omp*	acagctttagagacccctttgg	atccgagtgaggcagagttg	107.9
oxytocin receptor	*Oxtr*	acttagggcaagctggttga	cctgggtccaaaaatgacac	98.5
solute carrier family 32 member 1	*Slc32a1*	tgagggtggccagatttc	cctcctgctaaaccatgacc	103.6

Supplemental table 1. Genes, primer sequences and primer efficiency calculation, related to Fig.S4.